12-2004

Acoustic Wave Based Biosensor

Aditya A. Vijh
Western Michigan University

ACOUSTIC WAVE BASED BIOSENSOR

by

Aditya A. Vijh

A Thesis
Submitted to the
Faculty of Graduate College
in partial fulfillment of the
requirements for the
Degree of Master of Science
Department of Electrical and Computer Engineering (Electrical)

Western Michigan University
Kalamazoo, Michigan
December 2004

ACKNOWLDEGEMENTS

I would like to extend my heartiest gratitude to my advisor Dr. Massood Z. Atashbar for all the support and encouragement I received from him during my stay in Western Michigan University. He has been a constant source of inspiration and my interactions with him during the last two years have been invaluable. His guidance and experience have been instrumental in completion of my thesis.

I am indebted to Dr. Bruce Bejcek for letting me work in his laboratory and giving me hands on experience in biotechnology. He has been extremely helpful and my discussions with him have been a great source of knowledge.

I am also greatful to Dr. Gesink for being on my committee and reading my thesis. His suggestions have been really valuable.

I am thankful to the US Department of Defense (DOD) for supporting this work under contract number W81XWH-04-10250.

Special thanks are due to my friend Srikanth Singamaneni for all the help he provided me during my experiments. His supportive presence and suggestions are valued and cherished. I also want to thank Shakil Hossein, Michael Simpeh, Sridevi Krishnamurthy and Denise Smith for their encouragement and support during the completion of my thesis.

Thanks to my friend Ruchi Rai and my brother Manik Kapoor for bearing with me whenever I was cranky and for all the early morning tea and coffee they gave me.

Last but not the least I would like to dedicate my thesis to my parents. Thanks Mom and Dad for showing your confidence in me and being there whenever I needed you the most.

Aditya A. Vijh

ACOUSTIC WAVE BASED BIOSENSOR

Aditya A. Vijh, M.S.E.

Western Michigan University, 2004

Quartz Crystal Microbalances (QCMs) have been widely used for detection of various chemical and biological species in liquid media. In this work an improved binding of Protein A and IgG molecules on QCM biosensors by modifying the gold surface of the quartz crystal with an ultra thin polystyrene film followed by an acidic treatment has been reported. Protein A and IgG immobilizations on quartz crystals with the polystyrene film represented a 65% increase and a 40% increase respectively when compared to immobilization done directly onto the crystals. Atomic Force Microscopy (AFM) has been used to investigate and study the biomolecular coverage on different substrates. The results obtained using QCM and AFM are analyzed and correlated together. Simulation and modeling of the acoustic wave sensors is done using ANSYS 6.1 to enhance the understanding of the sensing phenomena and the design parameters of the sensor.

TABLE OF CONTENTS

Table of Contents- Continued

Table of Contents- Continued

LIST OF FIGURES

List of Figures- Continued

List of Figures- Continued

1. INTRODUCTION

Development of Micro Total Analysis Systems (μ-TAS) has revolutionized the world of micromachining technology. Recently research has been concentrated on developing biological microelectromechanical systems (bio-MEMS) and the so called "Lab on a Chip (LOC)" wherein the biological system is reduced down to the micro levels. These microelectronic systems can be easily integrated with the on chip electronics making large arrays of these systems possible. They can be of very low cost and easily packaged.

1.1 Biosensors

Biosensors are analytical devices that measure the interaction of biomolecules by converting a biological response to a detectable electrical signal. They consist of three different components (Figure 1-1). These components include the biological element to be tested (antibody-antigen pair, enzymes, bacteria etc), the transduction system and the detection system.

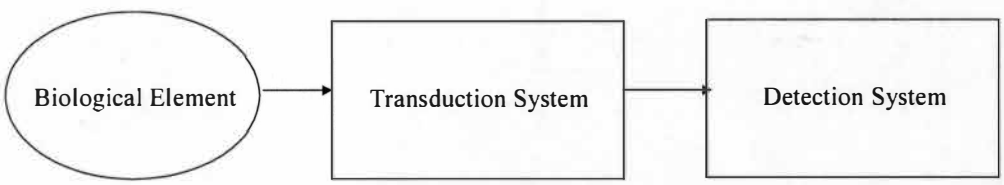

Figure 1-1: Biosensor configuration.

Some of the major considerations while designing a biosensor include:

- Immobilization of the biological element without affecting their biological activity.
- Selection of a suitable transduction method.

- Accuracy and repeatability.
- High sensitivity and selectivity for the target analyte.
- Insensitivity to variations in temperature, pH, pressure, viscosity, concentration, electrical and other environmental interferences.
- Portability.
- Low cost.

1.2 Types of Biosensors

Biosensors can be classified based upon the type of the transduction system. This transduction system may be piezoelectric, amperometric, potentiometric, calorimetric and optical.

1.2.1 Piezoelectric Biosensors: Piezoelectric biosensors consist of a piezoelectric substrate that oscillates at a resonant frequency on application of an electric field. Binding of any substance on the surface of the substrate causes a shift in the frequency of operation proportional to the amount of mass adsorbed.

1.2.2 Amperometric Biosensors: Amperometric biosensors detect the analyte by measuring the current change that occurs due to the transfer of electrons between the biomolecule and an electrode.

1.2.3 Potentiometric Biosensors: Potentiometric biosensors use ion selective electrodes to convert a biological reaction into an electrical signal and measure the potential at constant (ideally zero) current.

1.2.4 Calorimetric Biosensors: Calorimetric biosensors determine the analyte concentration by measuring the heat generated during an antigen-antibody reaction. The heat generated is measured using thermistors under closely monitored conditions wherein most of the heat generated may be registered as the temperature change.

1.2.5 Optical Biosensors: In optical biosensors light is made to pass through the biomolecular layer adsorbed on the surface of the sensor. The biomolecules absorb certain wavelength of the incident light. The reflected light is measured and the difference in the spectrum of the incident and the reflected light determines the concentration of the target compound.

The work presented here involves the usage of Quartz Crystal Microbalance (QCM), a piezoelectric acoustic wave biosensor to detect various concentrations of mouse immunoglobulin G (IgG) bound to the surface of the sensor. Further various modification techniques of the sensor surface have also been discussed resulting in much higher and improved binding of the biomolecules to the surface of the sensor.

1.3 Acoustic Sensors

Acoustic wave sensors have been widely used for many applications in detecting chemical and biological components in liquid media. By using the so-called chemical interfaces, they can be implemented for determining the concentration of a highly specific target compound in a liquid environment. The interface selectively adsorbs materials in the solvent to the surface of the sensing area. This adsorption results in the changes in the electrical and mechanical properties of the device which in turn causes changes in the acoustic wave characteristics namely amplitude and velocity and hence the

resonance frequency of the device. These changes in the acoustic properties of the sensor can be directly related to any mass change on the sensor surface.

1.4 Mass Sensitivity of Acoustic Sensors

Mass sensitivity is a criterion for acoustic sensor design. The mass sensitivity is defined as the incremental signal change occurring in response to an incremental change in mass per unit area of the surface of the device. For bulk wave resonators mass sensitivity is defined as [1]

$$S_m = \lim_{\Delta m \to 0} \frac{(\Delta f / f_0)}{\Delta m} \qquad (1)$$

where Δm is the per unit area mass uniformly distributed on the surface of the device, f_0 is the resonant frequency of the device and Δf is the change in the working frequency that occurs due to mass loading. Mass sensitivity for surface acoustic wave (SAW) devices is defined as [1]

$$S_m = \lim_{\Delta m \to 0} \frac{(\Delta V / V_0)}{\Delta m} \qquad (2)$$

where Δm is the per unit area mass uniformly distributed on the surface of the device, V_0 is the phase velocity and ΔV is the change in the phase velocity due to mass loading.

1.5 Types of Acoustic Sensors

1.5.1 Thickness Shear Mode (TSM) Resonators: The TSM resonators were first studied and used by Sauerbrey in 1959 [2] to determine the thickness of thin layers adhering to the surface of the device. Over the period of time, the usage of TSM

resonators has been extended for detection of various chemical and biological species by coating the surface of the device with a suitable detection layer. Also referred to as the Quartz Crystal Microbalance (QCM), TSM consists of an AT-cut quartz crystal with thin film metal electrodes patterned on both sides forming a single electrical port (gold is the ideal choice for the electrodes). These devices fall in the category of bulk wave acoustic sensors as application of a voltage produces an electric field throughout the bulk of the device. The piezoelectric nature of quartz in turn causes this electric field to produce a shearing motion transverse to the normal of the crystal. The resonant frequency of the device is inversely proportional to the thickness of the crystal (which is half a wavelength thick) and is typically between 5 MHz to 10 MHz. Quartz Crystal Microbalances have been used extensively for protein sensing [3, 4] and gravimetric immunoassays [5, 6, 7, 8]. One of the advantages of using QCM is the small temperature dependence of the operating frequency on the ambient temperature. The electronic circuitry and the measurements associated with QCM are relatively simple and straightforward. Further these devices have a very high Q (quality) factor. The most serious limitation of these devices is the low sensitivity which is limited by the thickness of the crystal. Although the device's sensitivity can be increased by decreasing the crystal thickness, it makes the crystal much more fragile. Figure 1-2 shows the top and the side view of a typical QCM crystal.

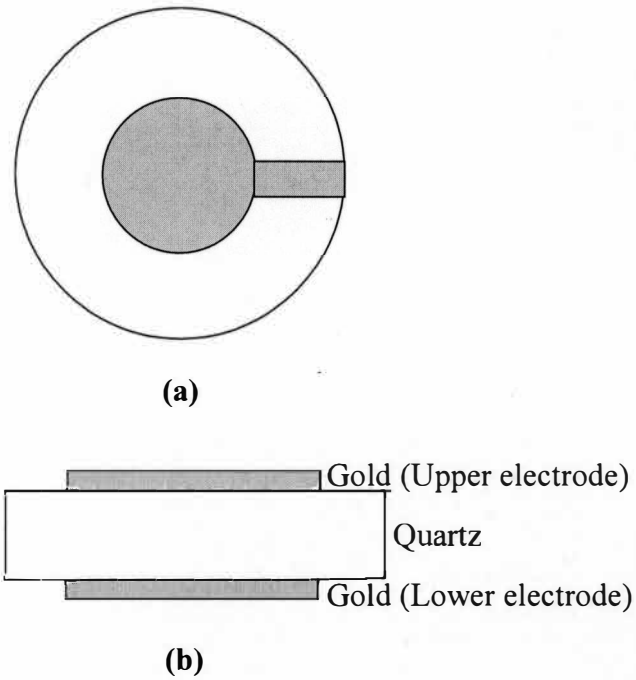

Figure 1-2: (a) Top view of a QCM crystal (b) Side view of a QCM crystal.

1.5.2 Surface Acoustic Wave (SAW) Sensors: Surface acoustic wave (Rayleigh) sensors consist of a piezoelectric substrate (quartz, lithium niobate, lithium tantalate etc) with electrodes patterned in the form of metal Interdigital transducers (IDT's). These sensors developed with the invention of IDT's [9] have wave energy confined mostly at the surface approximately one wavelength thick. The particles follow an elliptical path having displacements transverse to the direction of wave propagation and parallel and normal to the plane of the surface. The acoustic wavelength is determined by the IDT periodicity. These sensors are normally operated in a "delay line" configuration with one set of IDT's acting as a transmitter and the other set acting as a receiver. These devices work at higher frequencies (typical frequency of operation being 30-300 MHz) as compared to the TSM resonators and have higher sensitivity as the wave propagates not through the bulk of the device but near the surface in the region having thickness lower

than the operating wavelength. SAW sensors have found extensive usage in gas sensing [10, 11, 12] and biosensing applications [13, 14, 15]. The top and side view of a SAW is shown in Figure 1-3.

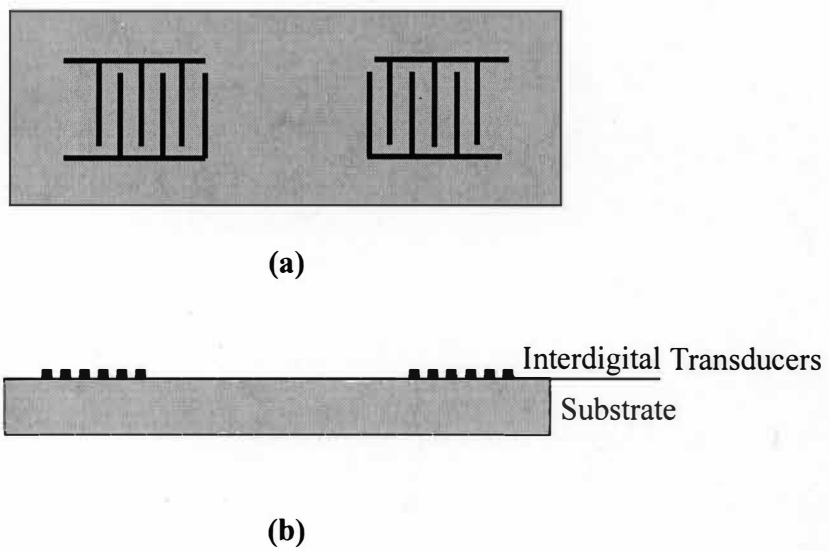

Figure 1-3: (a) Top view of a SAW sensor (b) Side view of a SAW sensor.

1.5.3 Shear-Horizontal Surface Acoustic Wave (SH-SAW) Sensors: SH-SAW sensors belong to the category of SAW sensors wherein the application of a potential to the IDT's produces an acoustic wave having particle displacement perpendicular to the direction of wave motion and in the plane of the crystal (shear displacement). As in SAW devices, the acoustic wavelength is determined by the transducer periodicity. SH-SAW sensors have been applied to a number of enzyme detection [16] and liquid sensing applications [17, 18].

1.5.4 Shear-Horizontal Acoustic Plate Mode (SH-APM) Sensors: SH-APM sensors [19, 20] are essentially Rayleigh sensors with a difference that the substrate thickness in these sensors is less than that in the SAW delay line devices. Under such conditions,

IDT's in addition to the Rayleigh waves generate the shear horizontal waves also. These waves travel are not confined to the surface only but travel through the bulk getting reflected between the top and the bottom surfaces of the substrate which now acts as an acoustic waveguide. The particle displacement for SH-APM devices is parallel to the surface (in plane) and transverse to direction of wave propagation.

1.5.5 Love Mode Acoustic Wave Sensors: Love Mode Acoustic Wave Sensors also referred to as Surface Skimming Bulk Wave (SSBW) sensors or Guided SH-SAW is essentially SH-SAW sensors with an acoustic waveguide or a guiding layer [21, 22]. An essential condition for existence of love waves is that the shear acoustic velocity in the guiding layer should be less than the shear acoustic velocity in the substrate. Under such conditions the elastic waves generated in the substrate get coupled to this surface guiding layer which traps the acoustic energy near the surface of the device thereby increasing the sensitivity of the device to mass loadings. Hence the guiding layer should be the one with low density and low shear velocity. The guiding layer also serves the purpose of passivating the IDT's from the contacting liquid [22]. The most commonly used substrates for SH-SAW sensors and Love mode devices are quartz, lithium niobate ($LiNbO_3$) and lithium tantalate ($LiTaO_3$). The guiding layer may be SiO_2 [23, 24, 25], certain polymers like Poly (methyl methacrylate) also known as PMMA [26] or ZnO [27]. The top and side view of a Love wave sensor is shown in Figure 1-4.

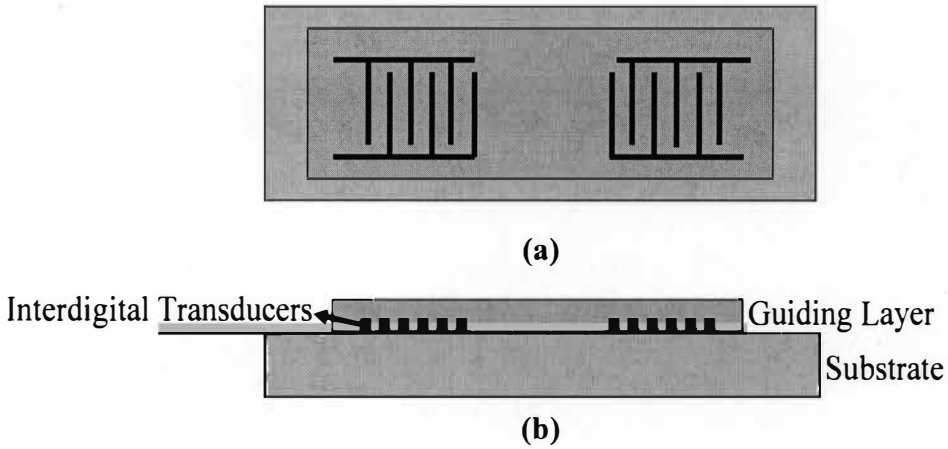

Figure 1-4: (a) Top view of Love wave sensor (b) Side view of a Love wave sensor.

1.5.6 Lamb Wave Sensors: Lamb waves sensors are essentially Rayleigh wave sensors wherein the waves propagate in a plate (membrane) having thickness less than an acoustic wavelength. Particle displacement is transverse to the direction of wave propagation and is parallel and normal to the plane of the surface. Application of a potential across the electrodes gives rise to both symmetric and anti-symmetric plate modes. The lowest order anti-symmetric mode (A_0) of the lamb wave is known as Flexural Plate wave (FPW) and it is this mode that is used in liquid sensing operations [28]. The membrane is formed by depositing a layer of silicon nitride by chemical vapor deposition and then etching it from the backside to the desired thickness. A piezoelectric layer of ZnO is then deposited on the upper membrane surface. The IDT's forming a "delay line" launch the flexural plate waves that set the whole membrane into motion. The wave velocities and hence the frequency of operation of these devices therefore depends upon the plate material and its thickness. Figure 1-5 shows the top, bottom and the side view of a flexural plate wave sensor.

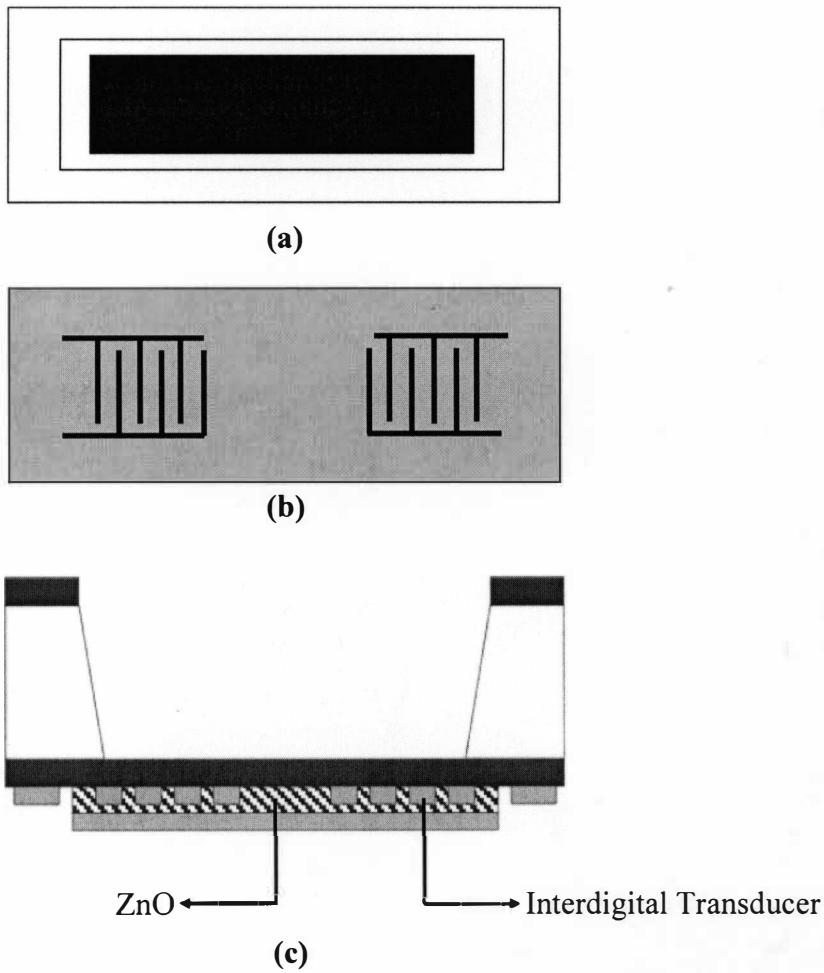

Figure 1-5: (a) Top view of a FPW sensor (b) Bottom view of a FPW sensor (c) Side view of a FPW sensor.

Strong radiation losses limit the use of longitudinal bulk modes and Rayleigh waves in a liquid environment. Therefore, acoustic modes, with no elastic coupling to the liquid such as TSM, SH-SAW, Love modes, and SH-APM are proper candidates for the development of devices to detect biomolecules in complex mixtures [29]. Acoustic wave devices use piezoelectric materials for the excitation and the detection of acoustic waves and hence the nature of almost all of the parameters involved with sensor applications concerns either mechanical or electrical perturbations. An acoustic device is thus sensitive mainly

to physical parameters, which may perturb the mechanical properties of the wave and/or its associated electrical field. For biological sensors, the binding of the antibodies and antigens on the substrate changes the mass of the membrane thus causing a drop in the wave velocity, which is correlated to the resonance frequency of the device.

2. FUNDAMENTALS OF IMMUNOASSAYS

2.1 Antibody

An antibody also referred to as *immunoglobulin* is a protein complex produced by the plasma cells to identify and specifically bind to a foreign substance known as an *antigen* and to neutralize it thus producing an immune response. Antibodies are broadly classified as *monoclonal antibodies* and *polyclonal antibodies*. Polyclonal antibodies are produced in the serum of an animal and are secreted against a specific antigen, each recognizing a different epitope. Monoclonal antibodies are produced by a single clone of cells and hence have specificity defined against only one affinity partner allowing for improved sensitivity and selectivity over polyclonal antibodies. The portion or the region on an antibody that binds to an antigen is referred to as an *epitope*.

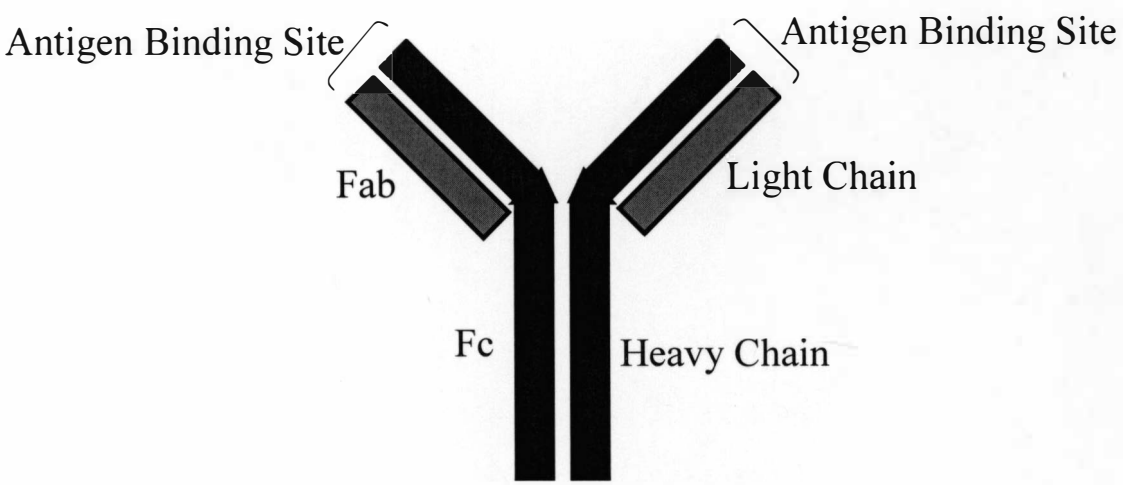

Figure 2-1: Structure of an antibody.

Figure 2-1 shows the basic structure of an antibody. Each antibody molecule has an approximate molecular weight of 150,000 Daltons (1 Dalton = 1.65 x 10^{-24} grams) and consists of two heavy chains and two light chains having molecular weights of 50,000 Daltons and 25,000 Daltons respectively. The stem of the Y shaped antibody molecule is referred to as the Fc fragment (fragment that crystallizes) whereas the two identical antigen binding fragments (Fab) form the V shaped portion of the antibody. Based upon the type of heavy chain antibodies are classified into five different subclasses namely IgA, IgD, IgE, IgG and IgM.

Immunoglobulin A (IgA) consists of 2 "Y" shaped molecules (dimer) and has therefore four epitope binding sites. It constitutes 6% of the total antibodies produced in the human immune system and has a half life of approximately 5 days. Immunoglobulin D (IgD) constitutes 0.2% of the serum antibodies and has a half life of 3 days. It is a monomer and therefore consists of only two epitopic site. Having a half life of approximately two days, Immunoglobulin E (IgE) constitutes upto 0.002% of the serum antibodies. Like IgD it is also a monomer having two epitope binding sites. The highest secreted of all the serum antibodies is the Immunoglobulin G which makes upto 80% of the serum antibodies. It consists of two epitopic sites and has a half life of 7-23 days. IgM is the first antibody produced by the immune system in response to any invasion. It constitutes 13% of the serum antibodies. It is a pentamer having ten epitopic sites and has a half life of approximately 5 days.

2.2 Immunoassay Techniques

This section describes the various immunoassay techniques currently in use. These immunoassays represent the various methods of specifically detecting immunoglobulins and their complexes formed with the affinity partners.

2.2.1 Radioimmunoassays (RIA): Radioimmunoassays use radioactive labels to detect the concentration of an antigen [30, 31]. The most commonly used radioactive labels are ^{125}I (Iodine) and ^{131}I. To start with a radioactively labeled antigen and antibody (against the antigen) are incubated together to form a complex. A known amount of an unlabeled antigen is then added to the mixture. This unlabeled antigen competes with the radioactively labeled antigen for the antibody epitopic sites and hence displaces some of the labeled molecules. A secondary antibody directed against the primary antibody (also known as anti antibody or α antibody) is then added to form a huge complex. The antibody-antigen-antibody complex is then centrifuged and the supernatant fluid is separated out. The supernatant fluid contains the unbound antigen whereas the centrifugate contains the bound antigen. The radioactivity of both the fractions is measured and the radioactive counts in the centrifugate when compared to the standard curves give the concentration of the unknown antigen. Figure 2-2 is a pictorial representation of the steps involved in radioimmunoassays.

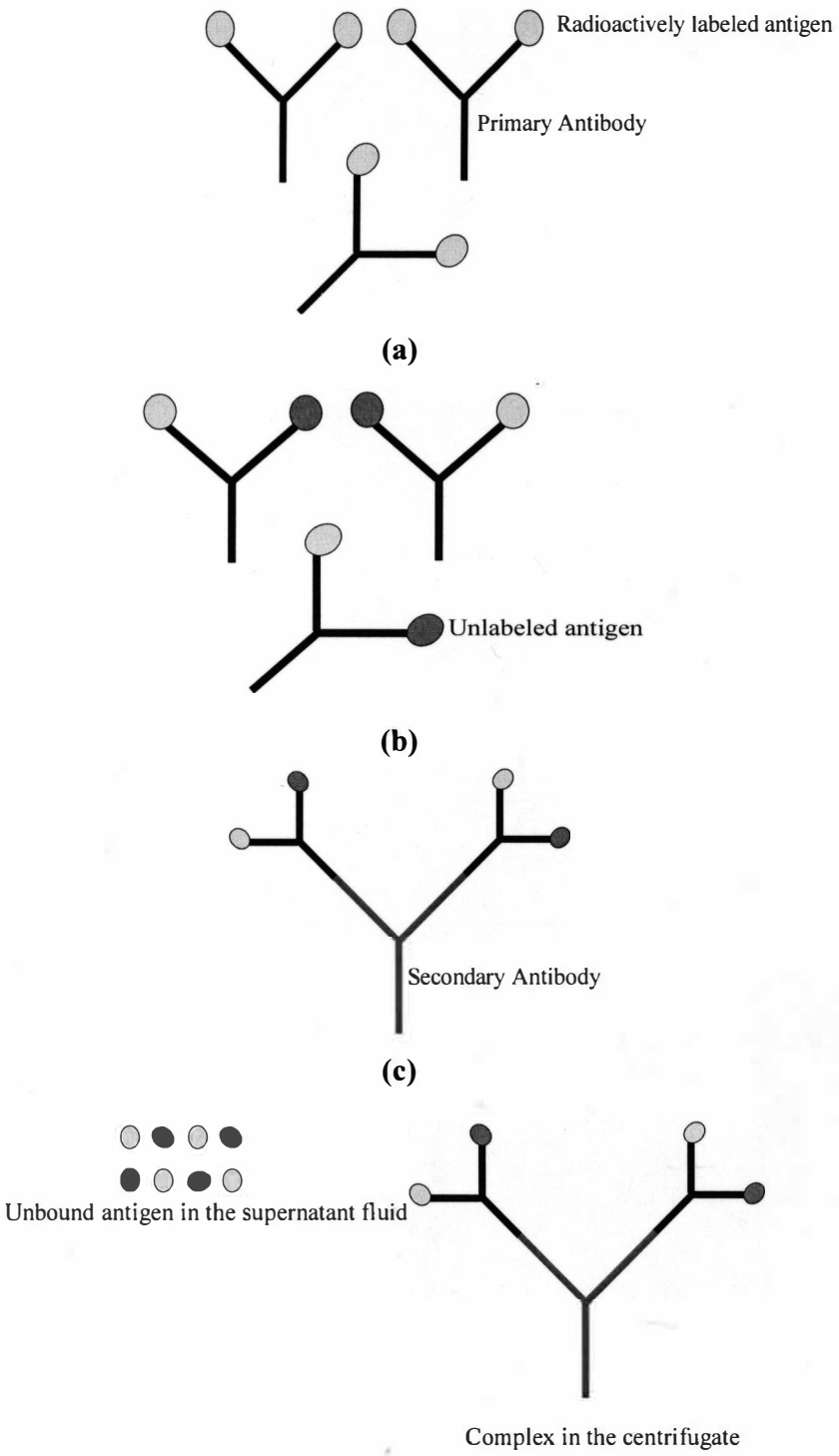

Figure 2-2: (a) Antigen-antibody complex (b) Addition of unlabeled antigen (c) Addition of secondary antibody (d) Centrifugation result.

2.2.2 Enzyme Immunoassays (EIA): Enzyme immunoassays use enzymatic labels which in the presence of an antigen catalyzes a reaction producing a product with a color change [32, 33, 34]. Enzyme immunoassays can be used for the detection of both the antigen and the antibody. The first step involves immobilization of the antigen specific antibody on a solid substrate. The antigen to be detected is then allowed to incubate with the antibody forming an antibody-antigen complex. An enzyme labeled antibody (against the same antigen) is then added to the sample mixture. Following its incubation a chromogenic substance is added which in the presence of the enzyme undergoes a change in color. The amount of the color developed gives an estimate of the amount of antigen present in the test sample. A pictorial representation of the steps involved in enzyme immunoassays is shown in Figure 2-3.

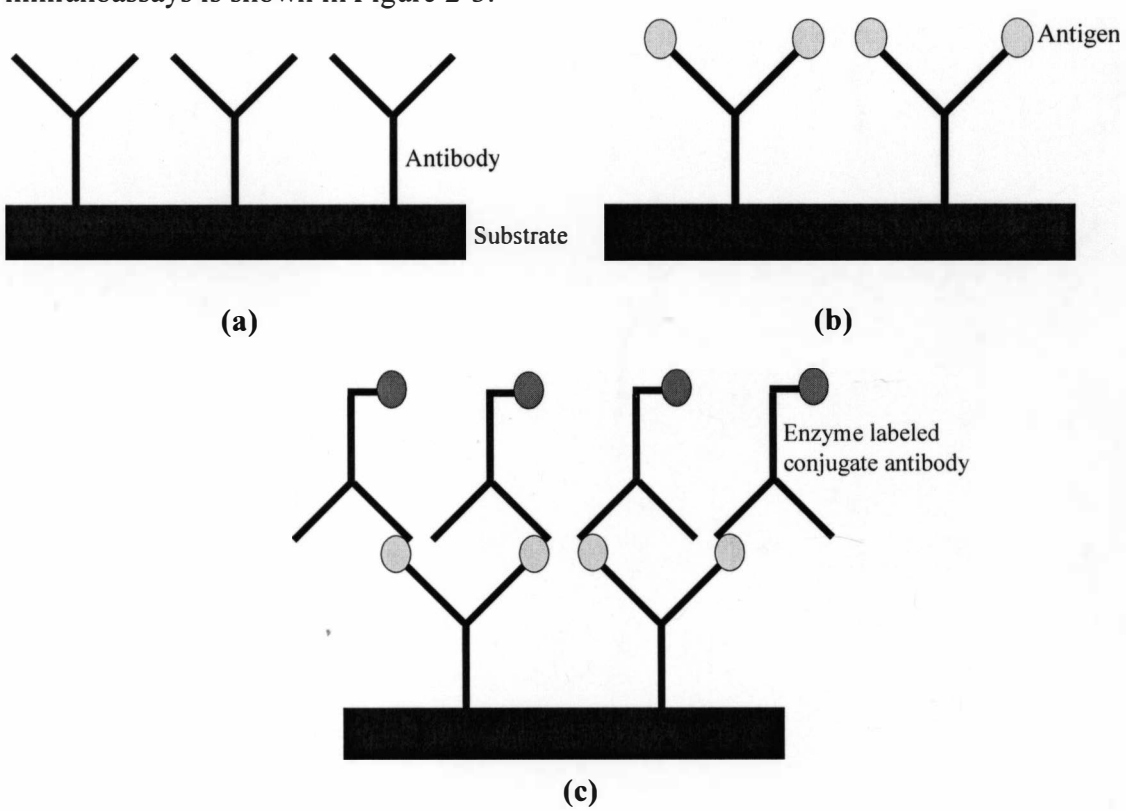

Figure 2-3: (a) Immobilization of the antibody on a solid substrate (b) Addition of the antigen (c) Addition of the enzyme labeled conjugate antibody.

2.2.3 Fluoroimmunoassays (FIA): Fluoroimmunoassays involve the usage of a fluorescent labels to detect the protein of interest [35, 36, 37]. When excited optically (at a specific wavelength) the labels emit fluorescent light. This light is then detected using fluorometers or fluorescent microscopes making the detection of biomolecules possible.

2.2.4 Chemiluminescent Immunoassays (CIA): These immunosassays use chemiluminescent labels to generate visible light from a chemical reaction [38, 39, 40] and differ from the fluoroimmunoassays by the fact that the labels used in these assays emit light when excited by a chemical reaction and rather than the light at excitation wavelength.

2.3 Advantages of Biosensors over the Current Immunosensing Techniques

Current immunoassay techniques suffer from the facts that they are cumbersome, laborious, expensive, and hazardous and require specific labels and reagents at individual steps of the detection process [41, 42]. Biosensors with rapid and highly sensitive detection capabilities for various biomolecules are therefore in great demand in the field of life sciences. These biosensors need no labels or distinct reagents and are much easier and simpler to implement. They can be made available as a handheld device and would be more economical than currently used technologies performing the complete testing and analysis of samples. This work therefore involves the usage of a QCM to specifically detect the amount of IgG bound to the surface of the sensor.

3. QUANTIZATION TOOLS AND METHODS

3.1 Quartz Crystal Microbalance (QCM)

A Quartz Crystal Microbalance (QCM) falls in the category of bulk acoustic wave sensors wherein the acoustic wave when excited flows through the entire bulk of the device. It consists of an AT-cut piezoelectric crystal sandwiched between two metal electrodes. Also referred to as a Thickness Shear mode resonator (TSM), the particle displacement in a QCM is perpendicular to the direction of wave propagation or in other words parallel to the sensing surface [43]. Figure 3-1 shows the cross sectional view of a TSM resonator indicating the direction of particle displacement (double headed arrow) and wave propagation.

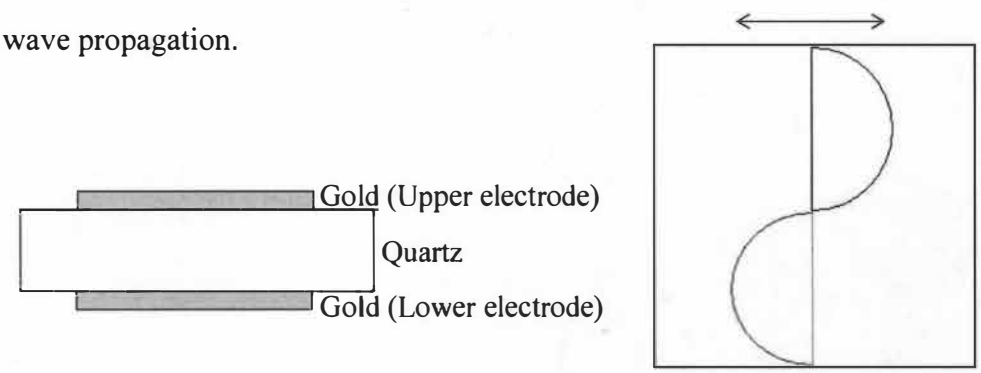

Figure 3-1: (a) Side view of the gold coated quartz crystal (b) Cross sectional view of the quartz substrate showing the direction of particle displacement and wave propagation.

Application of an alternating voltage potential across the quartz crystal by the two metal electrodes causes the crystal to oscillate at its resonant frequency. Figure 3-2 shows the basic electrical model of a quartz crystal resonator. The motional arm of the model

consists of a resistor (R), inductor (L) and a capacitor (C) in series. A capacitor C_0 is connected in parallel to the motional arm.

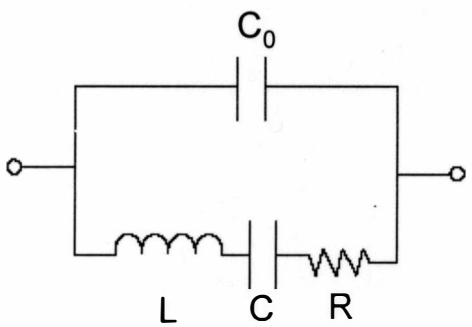

Figure 3-2: Electrical model of a QCM resonator.

Resistor R represents the losses induced in the resonator when the resonator is loaded with a viscous liquid. Capacitor C represents the elasticity of the quartz and its surrounding medium whereas the inductor L gives a measure of the mass added onto the crystal surface.

Figure 3-3 shows the oscillator circuit of the quartz resonator consisting of an automatic gain control (AGC) amplifier A and terminated in a load resistance R_L. The voltage across R_L is fedback to the input of the amplifier causing the circuit to oscillate at its resonant frequency (the frequency for which the phase shift around the loop is 0° or an integral multiple of 360°). Under conditions for which C_0 is zero, the resonant frequency (series resonance) for the circuit is given by the formula,

$$f = 1/2\pi\sqrt{LC}$$

For series resonance, the inductive reactance and the capacitive reactance cancel each other so the net reactance of the circuit is resistive. The circuit thus oscillates with a net loop gain of 1.

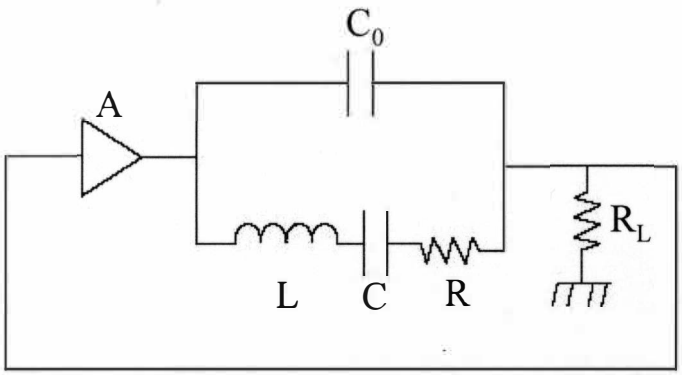

Figure 3-3: Quartz crystal oscillator circuit consisting of an amplifier A, quartz crystal resonator and a load resistance R_L.

The QCM used in my experiments was purchased from Stanford Research Systems (SRS) and had a resonant frequency of 5 MHz. The diameter of the crystal was 2.54cm and the thickness of the crystal was 331μm. The metallization layer consisted of gold (900nm) and chromium (18nm). The gold surface, which forms the active area for immobilization was 1.37cm^2 and the mass sensitivity of the crystal was 0.057 Hz/ng/cm^2. The short term stability of the crystal was 0.002 Hz (sec to sec). The upper and lower surfaces of the gold coated quartz crystal are shown in Figure 3-4.

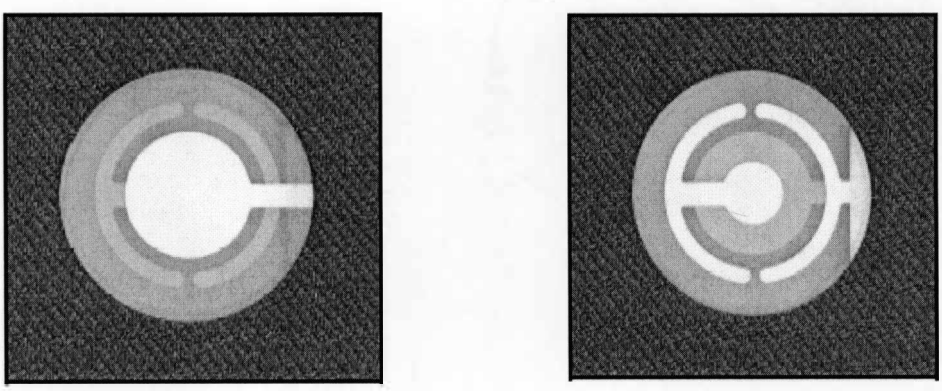

(a) **(b)**

Figure 3-4: (a) Liquid (Upper) surface of a QCM crystal (b) Contact (Lower) surface of a QCM crystal.

The setup used for our experiments is as shown in Figure 3-5. It consisted of a QCM25 crystal oscillator, QCM100 analog controller, SR620 universal time interval counter and a crystal holder.

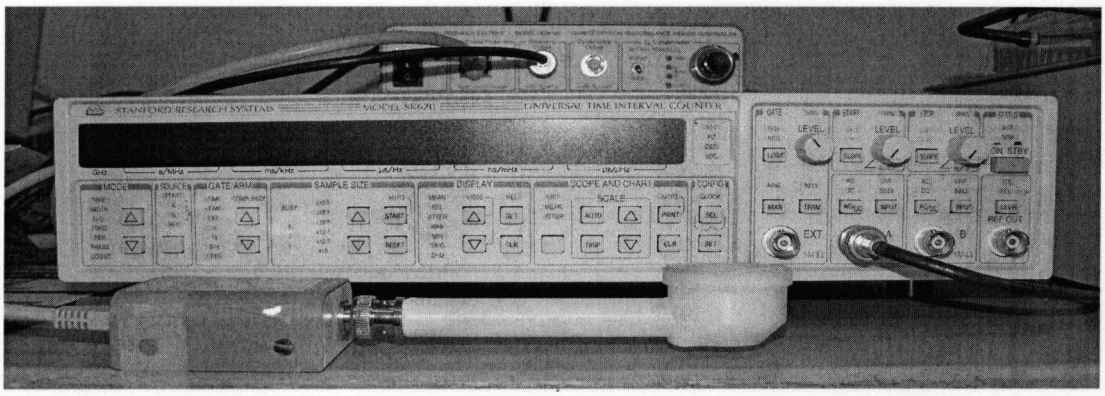

Figure 3-5: Experimental setup.

For practical applications C_0 is never zero. This causes a leading current to flow into R_L preventing the zero phase condition. It therefore is necessary to cancel C_0 in a way that the leading current through C_0 is cancelled by the lagging current through the motional arm. This is achieved by placing a varactor diode (having a variable capacitance) in the circuit as shown in Figure 3-6.

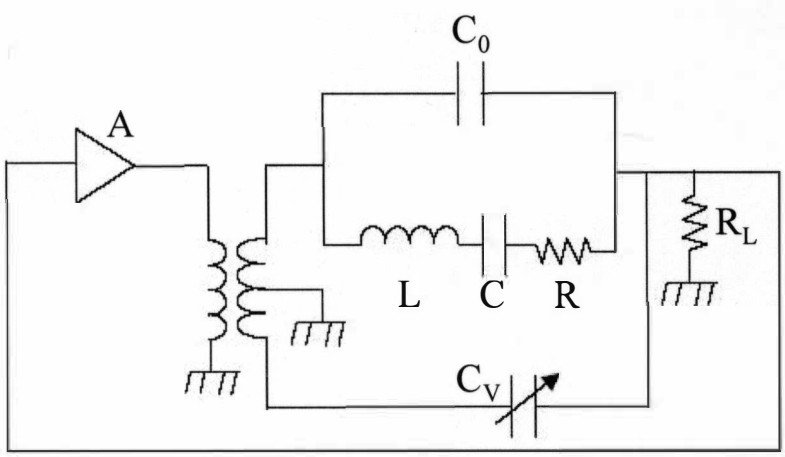

Figure 3-6: Quartz crystal oscillator circuit with nullified C_0.

The amplifier A drives a transformer with two secondary windings. One of the secondary windings drives the crystal resonator and the load. The other secondary winding (center tapped) inverts the voltage. With C_V connected in parallel with C, the net capacitance of the motional arm increases. The capacitive reactance decreases such that the net reactance of the motional arm becomes inductive. The inverted voltage drives the varactor to inject a lagging current into the circuit so as to cancel the current through C_0. The net reactance of the circuit thus remains resistive and the oscillations are sustained.

The QCM25 crystal oscillator maintains the 5 MHz oscillation of the crystal. It is connected to the QCM100 analog controller. The QCM100 analog controller powers up the QCM25 oscillator and provides a bias to the varactor to cancel C_0. The QCM thus oscillates at its series resonance frequency. The QCM25 and QCM100 are shown in Figure 3-7 and Figure 3-8 respectively.

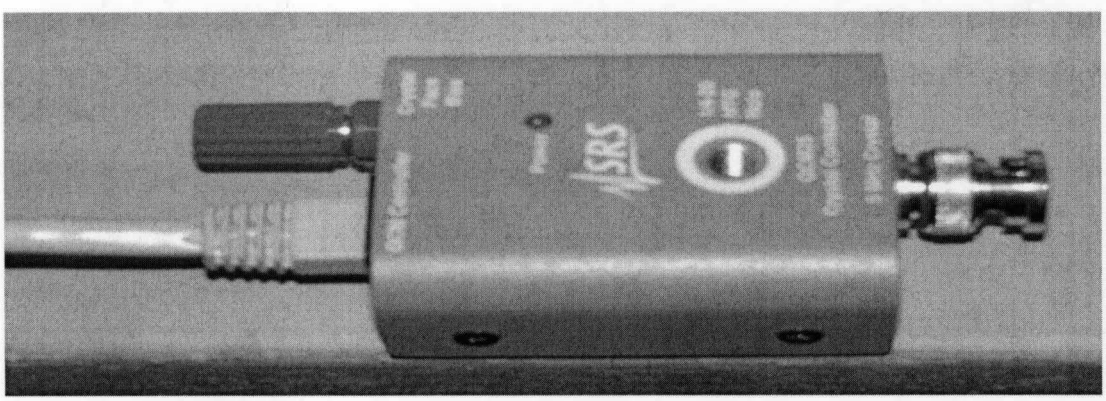

Figure 3-7: QCM25 crystal oscillator.

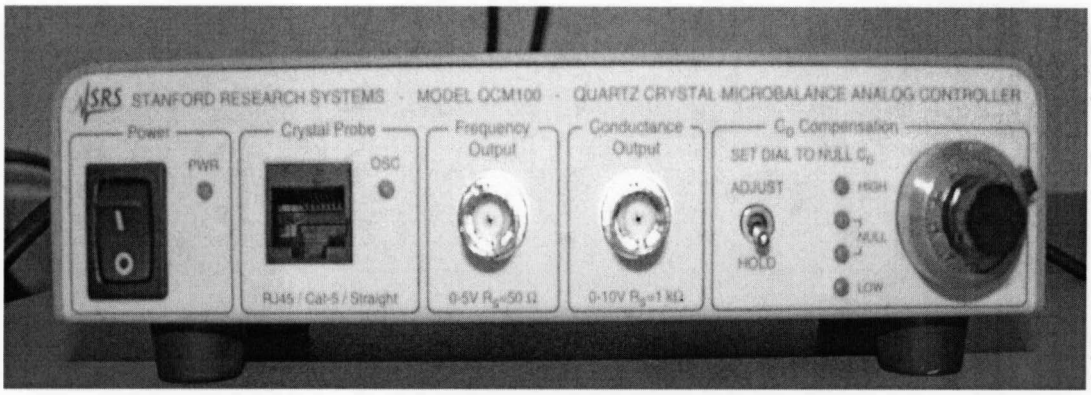

Figure 3-8: QCM100 analog controller.

The frequency measurements were done using a SR620 universal time counter (Figure 3-9) having a frequency range from 0.001 Hz to 1.3 GHz. The frequency and phase resolution of the device were upto 11 digits (Hz) and 0.001° respectively.

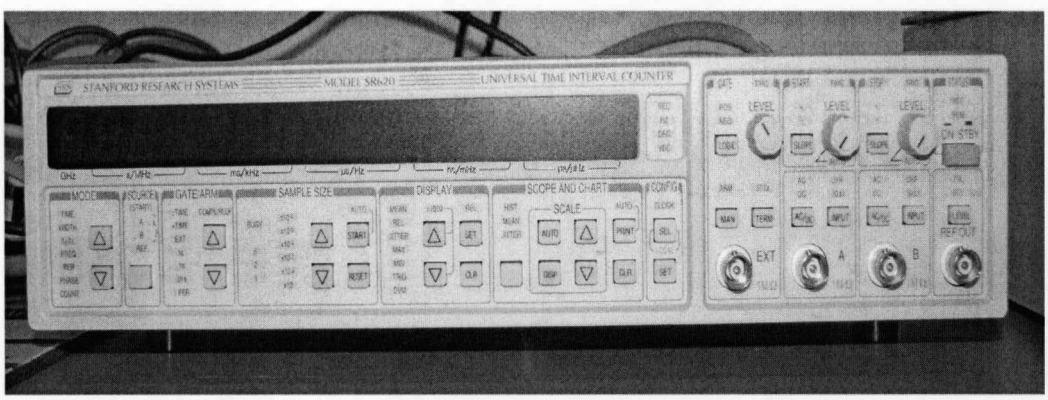

Figure 3-9: SR620 universal time counter.

Binding of the material onto the surface of the crystal causes the inductance L of the motional arm to increase. This results in a decrease in the resonant frequency of the device.

This change in the frequency (Δf) is related to the mass change (Δm) as per the Sauerbrey equation [44]

$$\Delta f = \frac{-2 f_0^{\,2} \Delta m}{A\sqrt{\rho_q \mu_q}}$$

where f_0= initial/ unperturbed resonant frequency.

A= piezoelectrically active area defined by the two gold electrodes.

ρ_q=density of quartz (2.648g cm^{-3}).

μ_q= shear modulus (2.947×10^{11} dyn cm^{-2}).

Sauerbrey equation is however based on an assumption that the mass has been uniformly and rigidly attached to the crystal and has negligible thickness as compared to the crystal as a whole [44]. Under such conditions the thin film acts as an extension of the quartz thickness and experiences no shear force during the crystal oscillation [44]. The simple relationship relating the change in frequency (Δf) to the change in mass (Δm) enables QCM to be widely used in sensing applications [45, 46, 47, 48].

3.2 Atomic Force Microscopy (AFM)

The Atomic Force Microscope (AFM) invented by Binnig, Quate and Gerber [49] consists of a ceramic/semiconductor tip mounted on a cantilever beam. The tip scans over the sample surface and a constant force is maintained between the tip and the sample. As the tip is repelled by or attracted to the surface, the cantilever beam deflects. The magnitude of the deflection is captured by a laser and a plot of the laser deflection versus tip position on the sample surface provides the topography of the surface.

3.2.1 Contact Mode of Operation: In the contact mode of operation the tip maintains a closed contact with the surface over which it is scanned. Under this mode the force on the tip is repulsive and has a mean value of approximately 1nN. As the tip and the sample remain in a constant contact, a strong lateral force is experienced by the sample resulting in its damage.

3.2.2 Non Contact Mode of Operation: In this mode of operation attractive Van der Waals forces exist between the tip and the sample as the tip is scanned 5-15 nm over the sample surface. The cantilever is oscillated at its resonant frequency. Usually a small AC oscillation is given to the tip to detect the weak attractive forces by measuring the changes in the amplitude, phase and frequency of the oscillating cantilever. As the tip is not in contact with the sample, the resolution is less compared to the contact mode. However, unlike the contact mode of operation the damage to the tip and the specimen is avoided.

3.2.3 Tapping Mode of Operation: In the tapping mode of operation the cantilever is made to resonate at a frequency of 50-500 KHz and brought close to the sample until a contact is made. Under such cases the tip contacts the sample for a very small fraction of its oscillation period. Tapping mode allows better quality imaging with high resolution and at the same time has little damaging effects on the sample.

In this work qualitative studies were made using Autoprobe CP Research AFM machine (Figure 3-10) in a non-contact mode. The AFM tips used for imaging were silicon with an approximate radius of curvature of 20nm. The AFM images were analyzed using image-processing software (IP 2.1) to calculate the RMS roughness value.

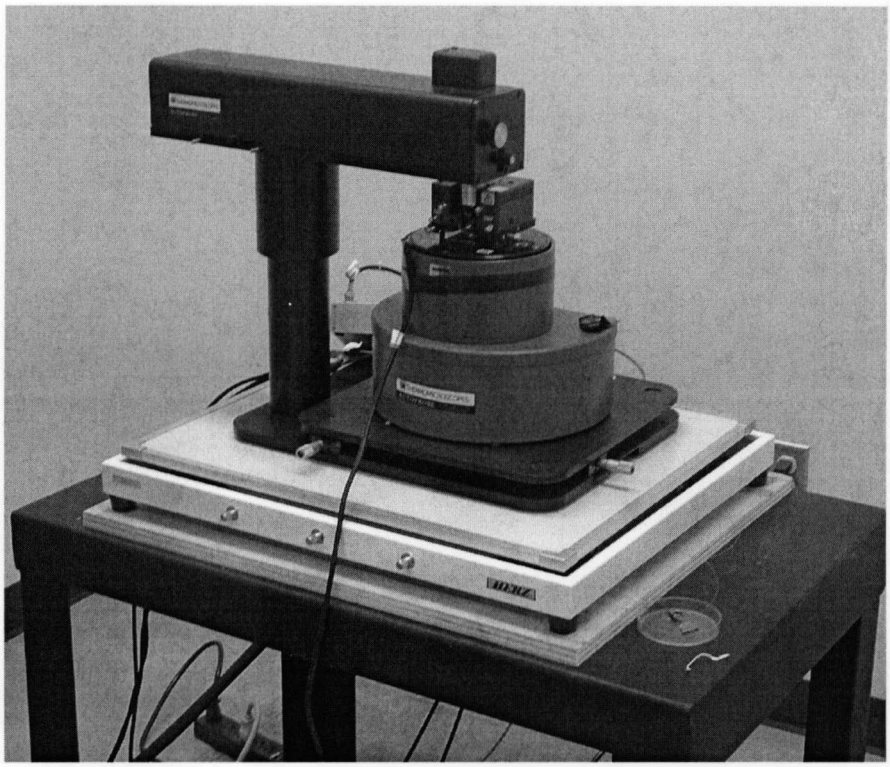

Figure 3-10: Autoprobe CP Research AFM machine.

3.3 Western Blot Analysis

Western Blot is a technique of separating proteins from a mixture of proteins depending upon their sizes. The protein identification is based on both antibody reactions and antigens. Proteins are separated on a denaturing sodium dodecyl sulfate (SDS) polyacrylamide gel and are transferred to a nitrocellulose/ PVDF membrane. The membrane is then exposed to solutions containing primary antibody, followed by a secondary antibody attached to an enzyme or a label. The membrane is subsequently soaked in a developer and a fixer solution to develop the color reaction, which results in identifying the antigen as a band. Prestained protein markers of known molecular weight are then used to measure the molecular weights of the visible bands.

4. ANTIBODY IMMOBILIZATION ON UNMODIFIED (BARE) GOLD SURFACE

This chapter discusses the methodology and the protocols adopted Muramatsu et al [50] to physically adsorb the antibody molecules on the surface of the gold crystal. The adsorption of the antibody molecules on the sensor surface was confirmed using a Quartz Crystal Microbalance and qualitatively studied using the Atomic Force Microscopy. Protein A (Sigma-Aldrich) and mouse monoclonal IgG antibody (BioDesign International Inc) were used throughout these studies. Glutaraldehyde and Glycine were purchased from Sigma-Aldrich. Glutaraldehyde acts as a cross linking agent between the chip and the biomolecules. Glycine is used as a blocking agent. Protein A was resuspended in phosphate buffered saline (PBS; Sigma-Aldrich) at a concentration of 500μg/ml. The mouse monoclonal IgG was resuspended in PBS and stored at -20^{0}C in aliquots. Aliquots were thawed and diluted to different concentrations as needed.

4.1 Preparation of the Gold Surface

Prior to the immobilization process the gold crystal was cleaned using Piranha solution (3 parts of H_2SO_4 in 1 part of 30 % H_2O_2) to remove any organic contamination from the surface of the crystal. Enough Piranha solution was employed to cover the gold surface of the chip and allowed to incubate at room temperature for two minutes. The chip was then thoroughly rinsed with milli-Q water. This procedure was repeated twice. The chip was subsequently blown dried in a stream of nitrogen gas.

4.2 APTES Modification of the Gold Surface

Gold has been found to be hydrophobic in nature and therefore causes the adsorbed biomolecules to denature and loose their activity. It therefore becomes essential to improve the hydrophilicity of the gold surface. This was achieved by the formation of a self assembled monolayer (SAM) of 5% 3-Aminopropyl triethoxysilane (3-APTES; Sigma-Aldrich) in acetone. Figure 4-1 shows the basic structure of an APTES molecule.

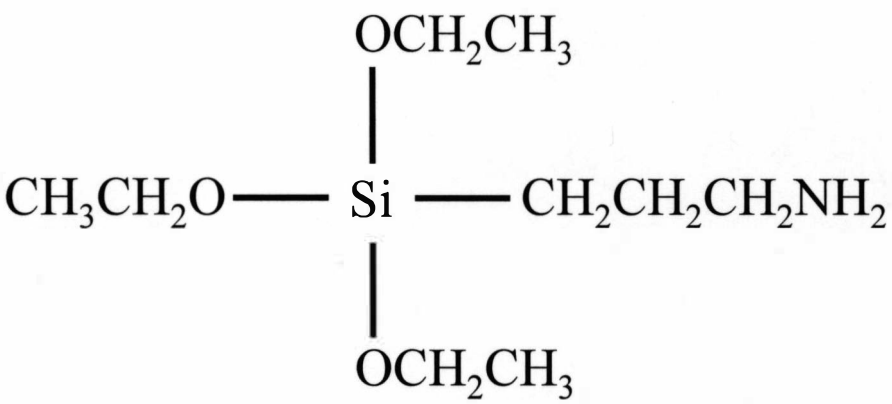

Figure 4-1: Molecular structure of APTES.

It is the presence of the terminal amine groups (NH_2) in APTES that is basically responsible for this improvement in hydrophilicity [50].

4.3 Protein A Incubation

After 1 hour following the APTES modification the chip was placed in a 5% (v/v) glutraldehyde solution (diluted in water) for 3 hours at room temperature to enhance the cross linking between the chip and the biomolecules. A 20µl solution of Protein A (500µg/ml; Sigma-Aldrich) resuspended in Phosphate Buffered Saline (PBS) was then immobilized onto the aldehyde modified surface for a period of 1 hour. Protein A having

a molecular weight of 45,000 Daltons was chosen because of its affinity towards the Fc fragment of the antibody thereby preventing the random orientations of the antibody molecules. The antibody orientation with and without the protein molecules are depicted in Figure 4-2a and 4-2b.

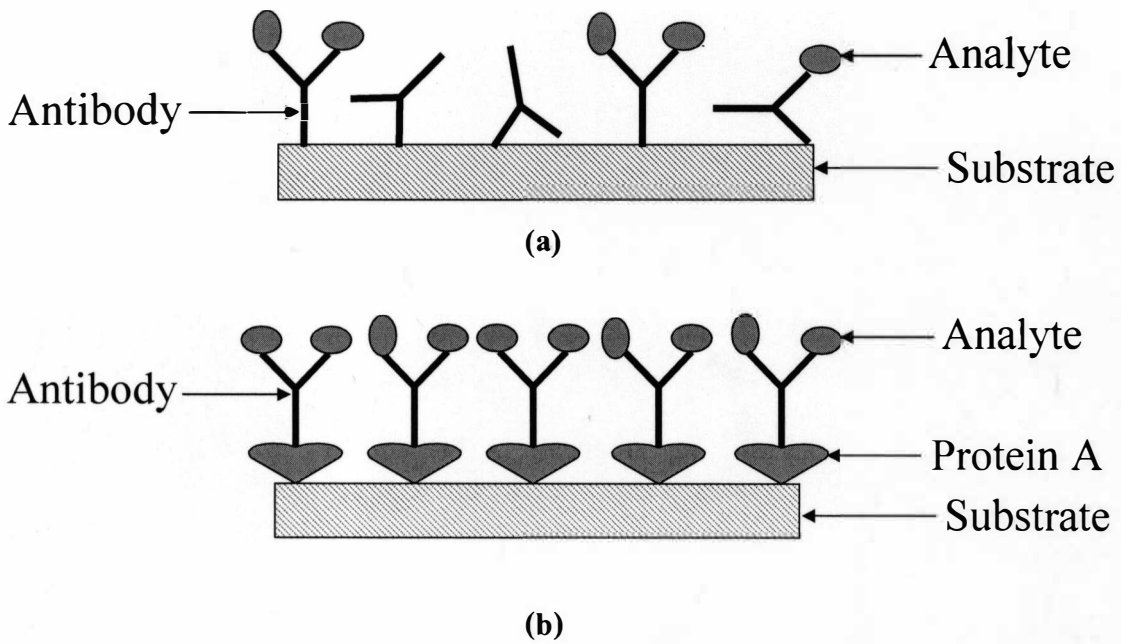

Figure 4-2: (a) Antibody orientation in the absence of Protein A (b) Antibody orientation in the presence of Protein A.

As can be seen from Figure 4-2, the presence of Protein A enables both the Fab fragments of the antibody molecule to be available for binding to the antigen resulting in an increase in the number of active sites. AFM image (Figure 4-3) revealed a uniform coverage of the surface with Protein A molecules of approximately 10nm in size. The scan size used was 1.6μm × 1.6μm.

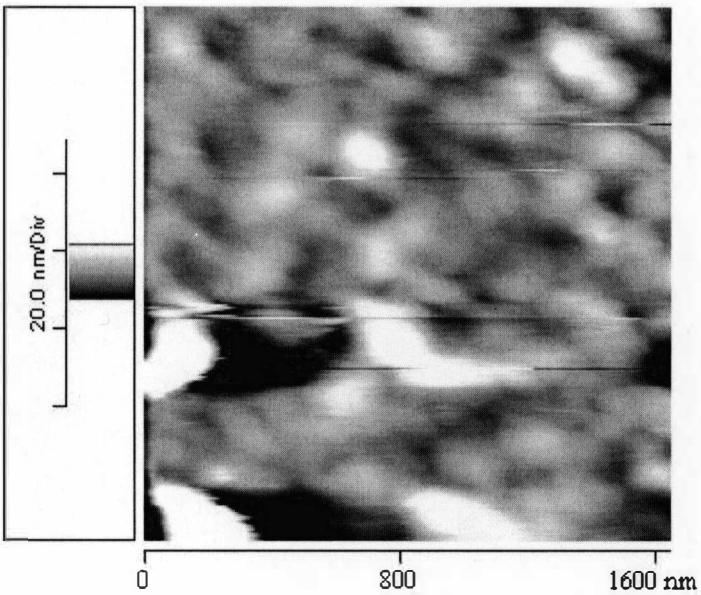

Figure 4-3: AFM image of immobilized Protein A.

Immobilization of Protein A on gold was then quantitatively studied with QCM. QCM when operated in liquids has been found to be sensitive to the viscosity and density of the liquid [51]. Under such conditions frequency shifts obtained using a QCM depend upon the absolute viscosity and density of the surrounding liquid as suggested by Kanazawa et al [52]. Changes in viscosity were avoided by maintaining a constant buffer environment of PBS on the crystal surface. Figure 4-4 represents the QCM frequency response to the protein immobilization. Point 1 in the figure refers to the point of addition of the Protein A containing solution to the chip. Point 2 indicates when the crystal was subjected to several wash-dry cycles and point 3 represents new resonance frequency of the crystal when Protein A was specifically bound on the surface. The frequency shift due to this direct binding (the difference in frequency between point 1 and point 3) was 220 Hz. From the Sauerbrey equation, this frequency shift corresponds to a binding of 2.8μg of protein.

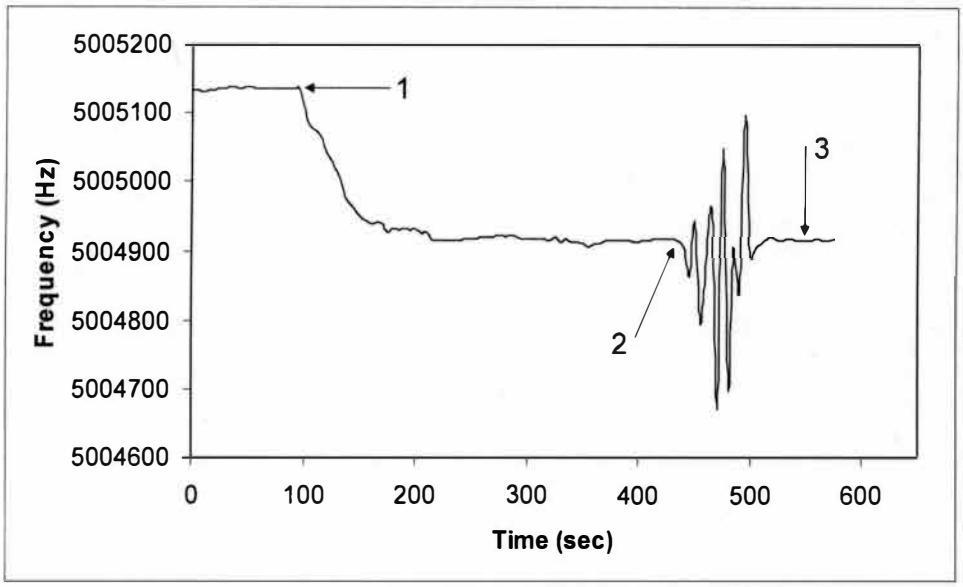

Figure 4-4: QCM frequency response to Protein A immobilization.

4.4 Antibody Immobilization

Following Protein A incubation the chip was covered with 0.1 M Glycine dissolved in PBS for 1 hour to block any sites not bound to Protein A on the glutaraldehyde modified chip. The crystal was then thorough rinsed with 0.1M Glycine-HCl buffer (pH 2.4) followed by milli-Q water to wash off any excess proteins or glycine. Different concentrations of the mouse monoclonal IgG antibody was then incubated on the chip for 1 hour followed by rinsing with 0.5M NaCl to remove any non-specifically adsorbed antibody. For antibody concentration of 80μg/ml, QCM registered frequency shift of 172 Hz corresponding to a mass change of 2.21μg (Figure 4-5). Point 1 indicates the time at which the antibody was added to the crystal. Point 2 represents the time when the crystal was rinsed with 0.5M NaCl to remove any non-specifically adsorbed IgG and point 3 corresponds to the final resonant frequency after the NaCl rinsing.

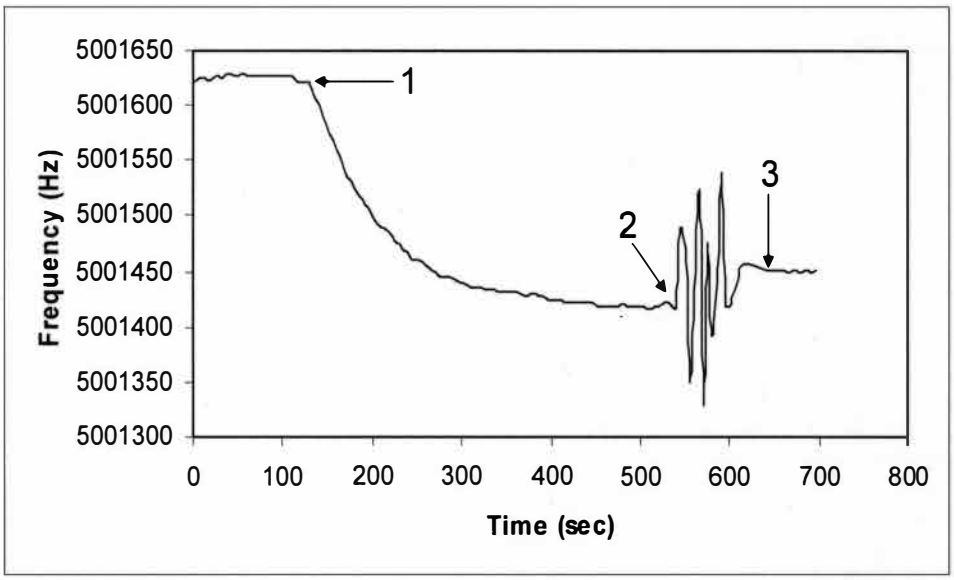

Figure 4-5: QCM frequency response to antibody concentration of 80μg/ml.

The QCM frequency shifts for antibody concentrations of 120μg/ml and 160μg/ml shown in Figure 4-6 and Figure 4-7 were found to be 205 Hz and 282 Hz for mass uptakes of 2.63μg and 3.62μg respectively.

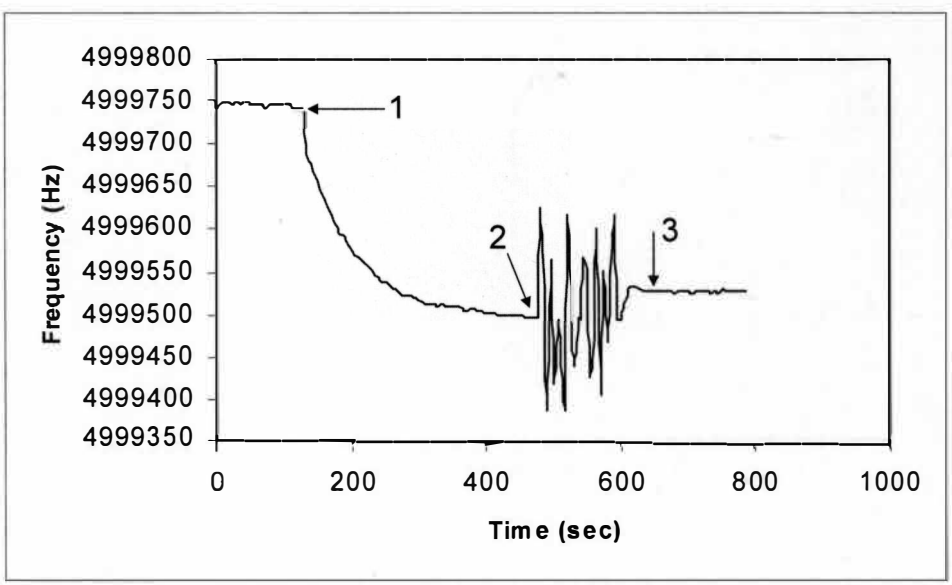

Figure 4-6: QCM frequency response to antibody concentration of 120μg/ml.

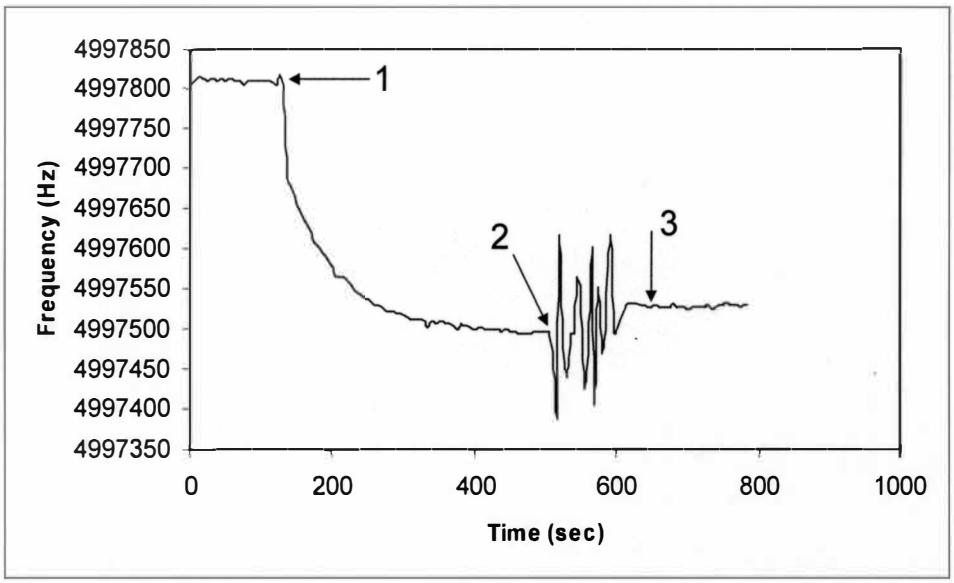

Figure 4-7: QCM frequency response to antibody concentration of 160μg/ml.

4.5 Summary

To conclude, antibody immobilization on APTES modified gold crystal was studied. APTES modification resulted in an improvement in the hydrophilicity of the surface which prevents biomolecules from getting denatured. Protein A was incubated onto the chip to prevent the random orientations of the antibody molecules. Protein A incubation resulted in a frequency shift of 220 Hz. Prior to antibody immobilization, Glycine was used to block the unoccupied sites on the glutaraldehyde modified surface. Mouse monoclonal antibody with different concentrations was then immobilized on the protein coated surface. Antibody with concentrations of 80μg/ml, 120μg/ml and 160μg/ml registered frequency shifts of 172 Hz, 205 Hz and 282 Hz respectively.

5. ANTIBODY IMMOBILIZATION ON POLYMER COATED GOLD SURFACE

This chapter describes the methodology and the protocols described in Chapter 4 to physically adsorb the antibody molecules on a polymer coated gold surface. The polymer used in our case was polystyrene. An improved binding of Protein A and IgG molecules on QCM biosensors by modifying the gold surface of the quartz crystal with an ultra thin polystyrene film followed by an acidic treatment was observed. This resulted in an appreciable increase in the frequency shift obtained using the QCM when the polystyrene film was used as an interfacial layer.

5.1 Preparation of the Ultra Thin Polystyrene Film

The gold surface was cleaned using Piranha solution as described in Chapter 4. For the experiments in which binding was measured with the polymer film, a 7% w/v solution of polystyrene (Sigma-Aldrich) in chloroform was spin coated onto the gold coated crystal at a speed of 1000 rpm. The second to second short term and the long term stability of the device following the polymer coating were found to be 0.004167 Hz and 0.004513 Hz respectively.

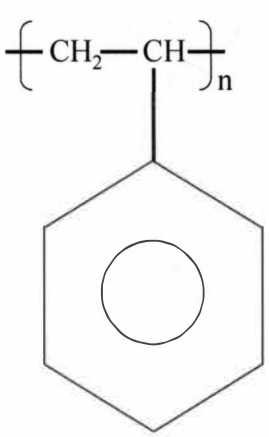

Figure 5-1: Structure of a polystyrene molecule.

Figure 5-1 shows the basic structure of a polystyrene molecule. It basically consists of a long hydrocarbon chain with phenyl group attached to each carbon atom. The AFM image of a polystyrene coated gold surface is shown in Figure 5-2. The scan size used for the AFM imaging was 5 μm × 5 μm.

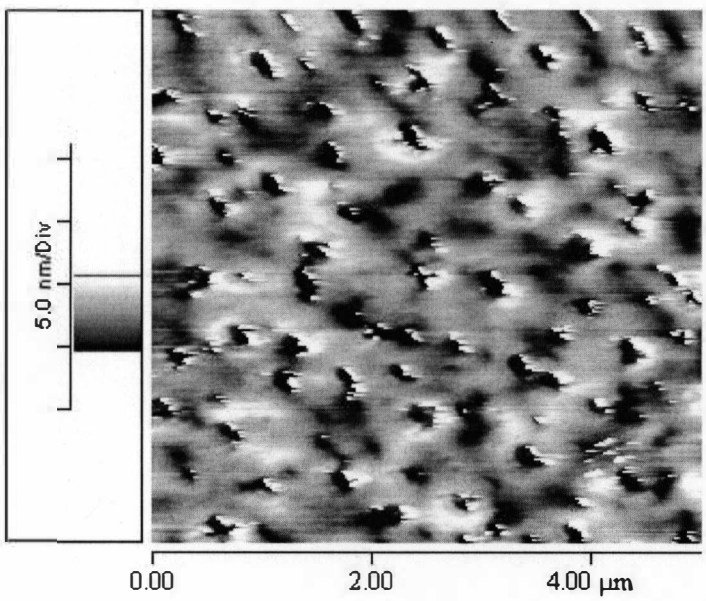

Figure 5-2: AFM image of a polystyrene coated gold surface.

5.2 APTES Modification of the Polystyrene Coated Gold Surface

Like gold, polystyrene is also hydrophobic. This hydrophobic nature of the polymer denatures the biomolecules resulting in a loss of their activity. To avoid denaturation of the biomolecules, the polymer film functional groups such as amino and hydroxyl groups can be chemically added. This helps the biomolecules retain their activity as immobilization now takes place through the hydrophilic arms of the polymer film [53, 54]. To increase the hydrophilicity of the surface which would increase the ability to add the functional groups, the chips were subjected to an acidic treatment followed by aqueous silanization using 3-APTES [55]. Figure 5-3 shows the schematic representation

of the acidic treatment and the APTES modification of polystyrene. The acid treatment provides NO_2 groups and the APTES modification improves the hydrophilicity of the surface by providing the required amine groups.

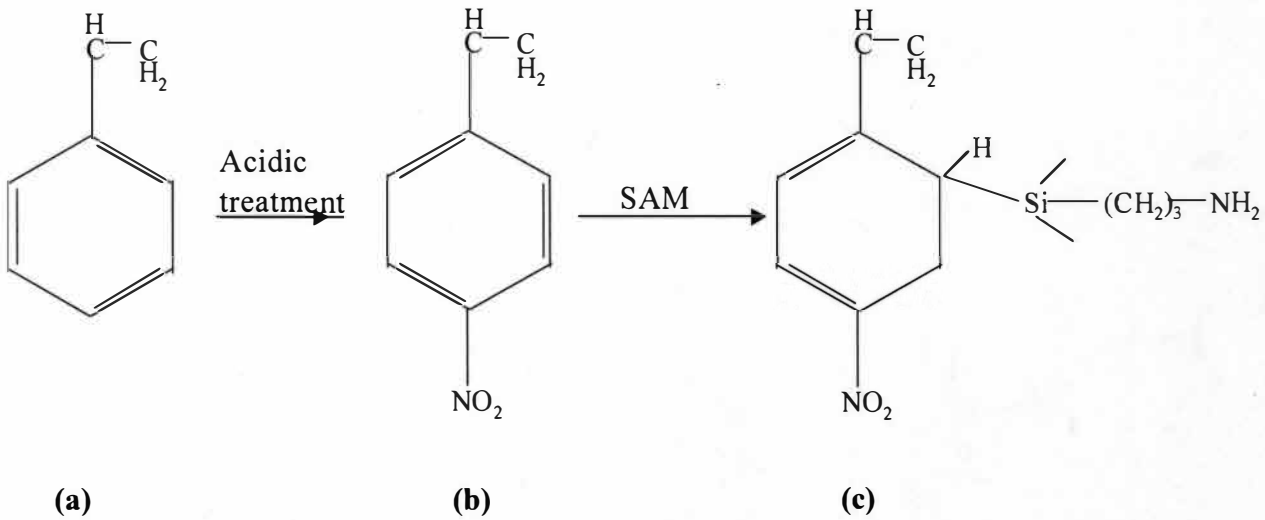

Figure 5-3: Polystyrene film when treated with acid and 3-APTES (a) Polystyrene film (b) Formation of the NO_2 groups by acidic treatment (c) Formation of the amine (NH_2) groups by silanization.

5.3 Confirmation of the Improvement in Hydrophilicity of the Polystyrene Coated Surface

This improvement in the hydrophilicity was confirmed by monitoring the distribution of water droplet on polystyrene and APTES modified polystyrene surfaces. Figure 5-4 shows the water distribution images (recorded using a Digital Blue Computer microscope) on polystyrene and modified polystyrene surfaces respectively.

(a)

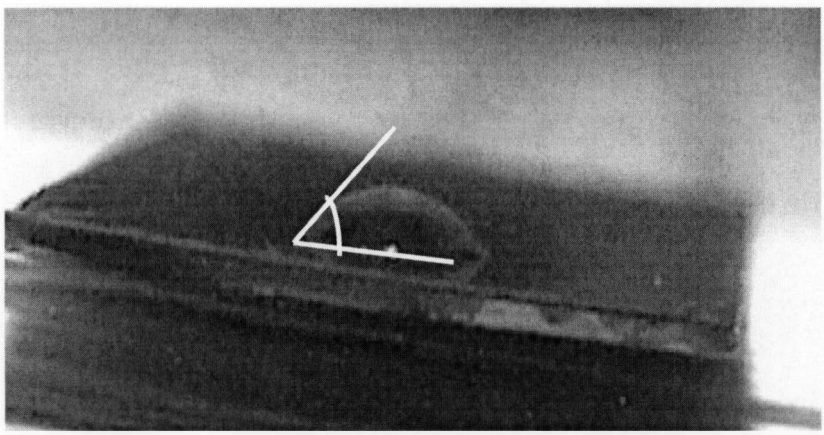

(b)

Figure 5-4: (a) Image of water distribution on polystyrene coated surface (b) Image of water distribution on APTES modified polystyrene surface.

A decrease in the contact angle of about 34° (from 89° to 55°) for APTES modified polystyrene surface was observed compared to the unmodified surface. A completely hydrophobic surface has been found to have a contact angle of 180° as compared to 0° for a completely hydrophilic surface. A decrease in the contact angle as observed in our experiment is therefore indicative of the improvement in the hydrophilicity of the APTES modified surface. The improvement in the hydrophilicity was further ratified with AFM

study of IgG molecules (approximately 10 nm in size) immobilized on APTES modified polystyrene surface (Figure 5-5).

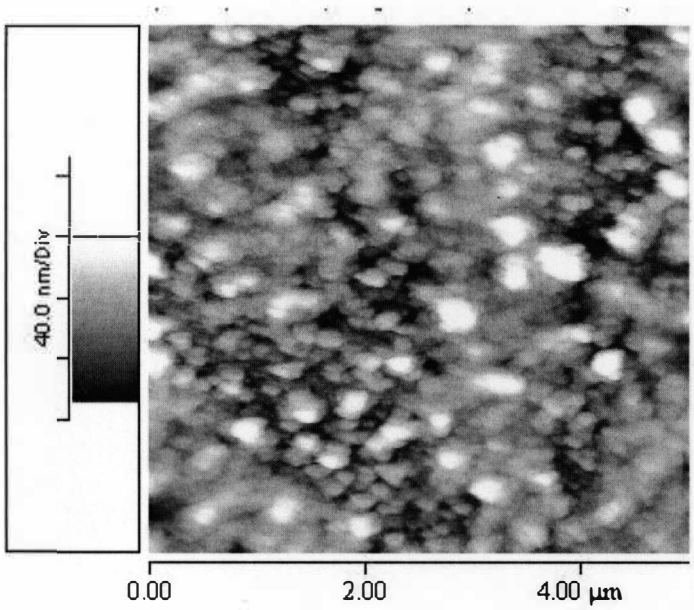

(a)

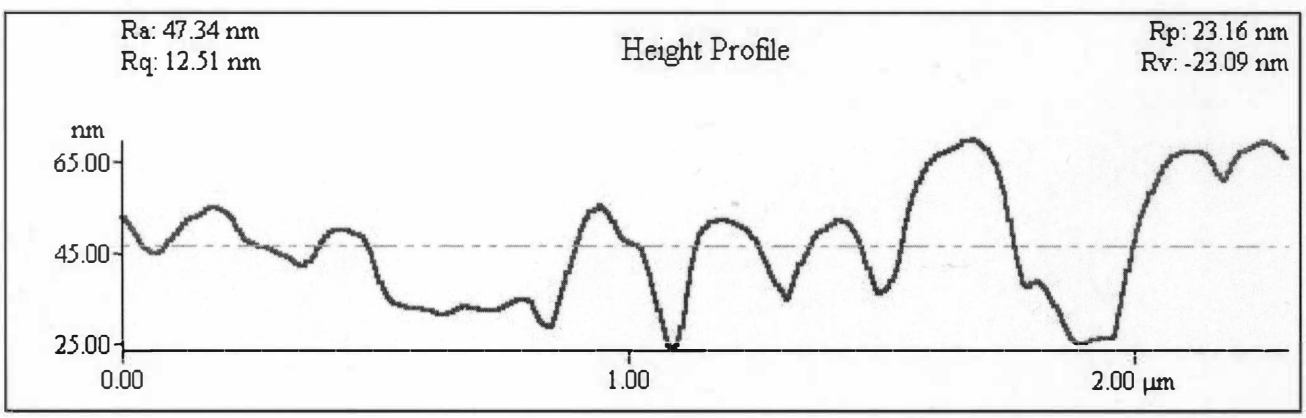

(b)

Figure 5-5: (a) AFM image of IgG immobilized on polystyrene coated surface (b) Height profile of the surface along a line.

A zoomed in image of the IgG immobilized on polymer modified surface is shown in Figure 5-6. The AFM imaging performed two hours after the biomolecular immobilization revealed that the molecules retained their characteristic "heart shape" indicating that they were not denatured.

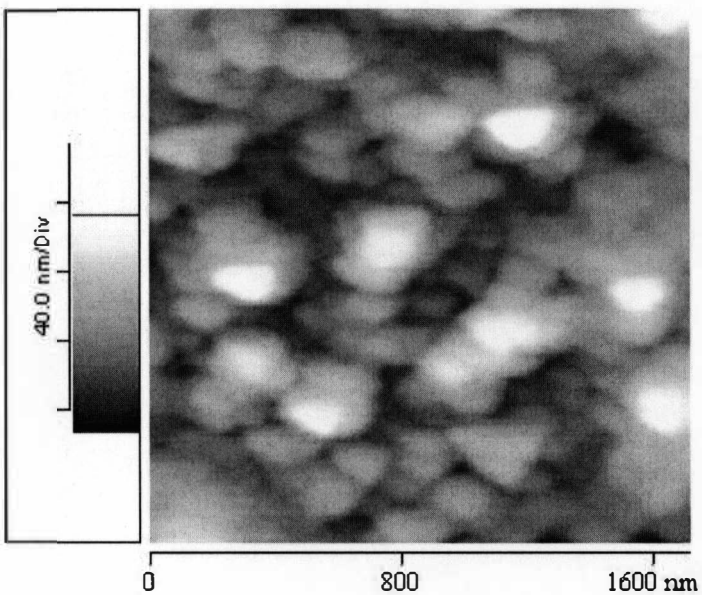

Figure 5-6: Zoomed in AFM image of IgG immobilized on polystyrene coated surface.

5.4 Protein A and Antibody Immobilization

Following the confirmation of improvement in the hydrophilicity of the polymer coated surface, the chip was treated with glutaraldehyde for a period of 3 hours. Protein A and mouse monoclonal IgG antibody were then incubated on the modified surface using the same protocols as described in Chapter 4. The QCM frequency response for Protein A immobilization is shown in Figure 5-7. The registered frequency shift from was 364 Hz which corresponds to a mass uptake of 4.66 μg. This represented a 65% increase in the frequency shift when compared to the QCM chips that were not coated with the polymer

film. As in previous experiments point 1 represents the instant when protein A was incubated onto the chip, point 2 is the time when the crystal was subjected to several wash-dry cycles of PBS and point 3 is the instant when the frequency stabilized corresponding to the specific binding of protein A.

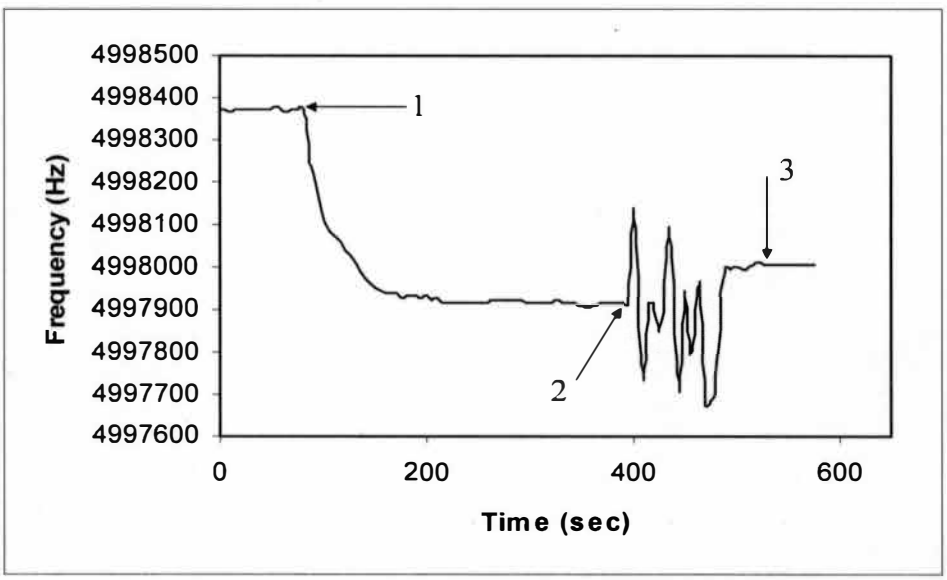

Figure 5-7: QCM frequency response to Protein A immobilization on polystyrene coated surface.

Similar results were obtained for the binding of IgG. The QCM response (Figure 5-8) for the immobilization of IgG (80μg/ml) on the polystyrene surface showed a frequency shift of 260 Hz. This represented a 40% increase in the frequency shift when compared to chips that had not been modified with polystyrene.

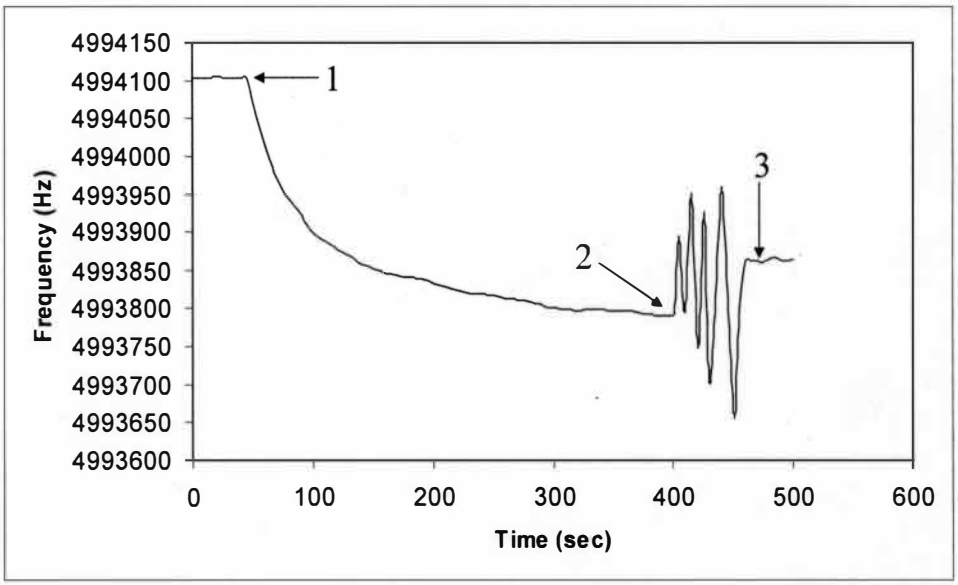

Figure 5-8: QCM frequency response to IgG (80 μg/ml) immobilization on polystyrene coated surface.

Similar to what was found with the antibody concentration of 80μg/ml, antibody concentrations of 120μg/ml and 160μg/ml also showed an approximate 40 % increase in registered frequency shifts (325 Hz and 391 Hz respectively) for immobilizations done on crystals coated with polystyrene. QCM frequency response for antibody concentrations of 120μg/ml and 160μg/ml is shown in Figure 5-9 and Figure 5-10 respectively.

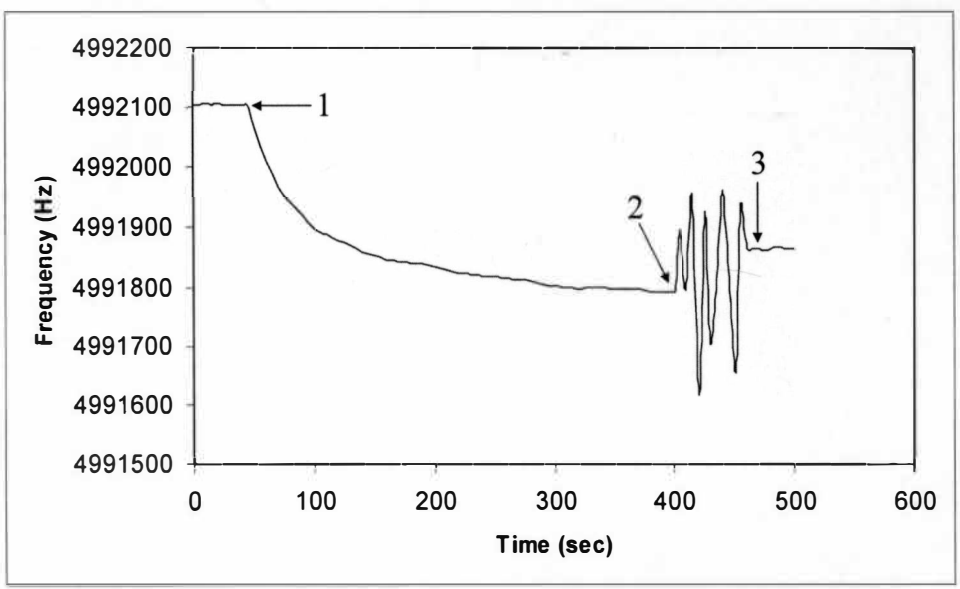

Figure 5-9: QCM frequency response to antibody concentration of 120μg/ml on polystyrene coated surface.

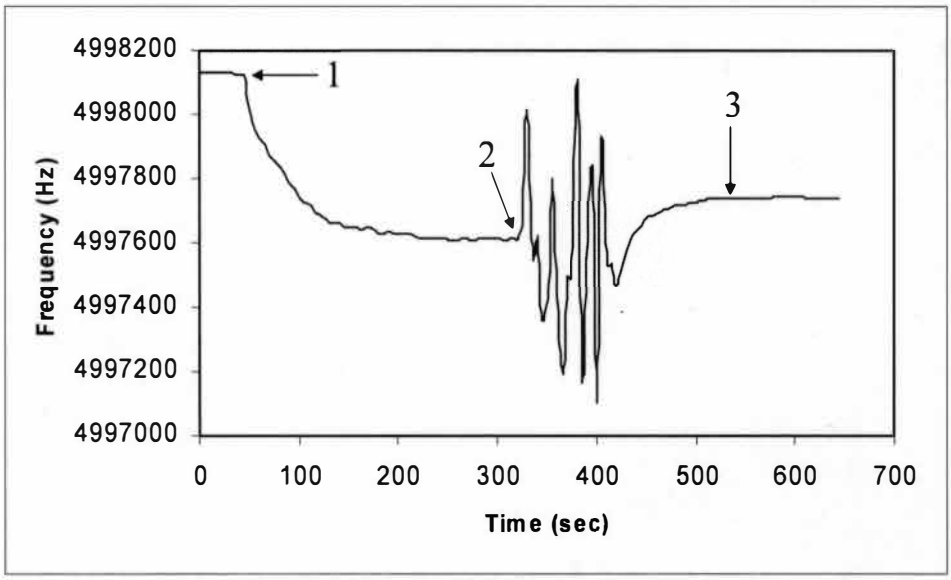

Figure 5-10: QCM frequency response to antibody concentration of 160μg/ml on polystyrene coated surface.

Figure 5-11 shows the frequency shifts and mass immobilized for different IgG concentrations with and without the polymer film modification. The upper set of curves represents the frequency shifts and the corresponding mass uptakes registered for immobilization carried on the polystyrene modified surface whereas the lower set of curves represents the frequency shifts and the corresponding mass changes registered for immobilization carried on bare gold surface. As is evident from Figure 5-11, an ultra thin film of polystrene aids in a higher and a much improved binding of biomolecules resulting in higher frequency shifts (40% increase) and hence higher mass changes.

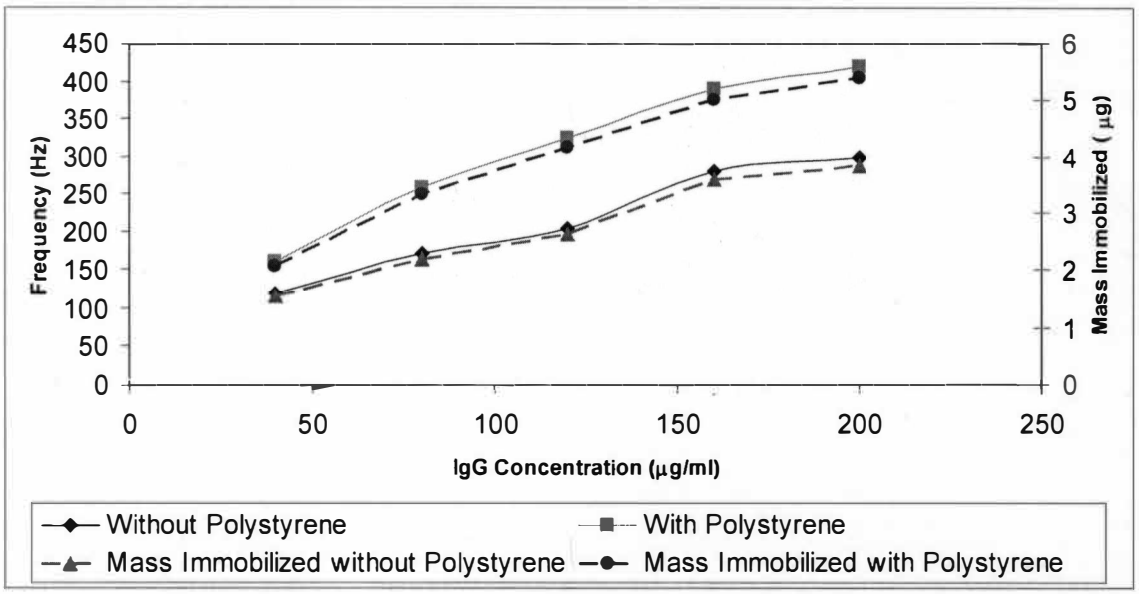

Figure 5-11: Frequency shifts and Mass immobilized for different IgG concentrations with and without polystyrene.

5.5 Discussion on Improved Biomolecular Binding and Increased Frequency Shifts

AFM images of the bare gold crystal and polystyrene coated crystal along with the height profile of the surface along a line are shown in Figure 5-12 and Figure 5-13 respectively. The AFM studies (as is evident from Figure 5-12) revealed that the gold coated quartz crystals had a RMS surface roughness of 98.4nm. An appreciable decrease in the surface roughness to 1.75nm was observed when the crystal was coated with an ultra thin layer of polystyrene. Gold and polystrene are both hydrophobic in nature. APTES modification of the gold surface although improves the hydrophilicity of the surface, it doesn't result in much decrease in the roughness of the surface. On the other hand APTES modification of the polystyrene coated surface not only improves the hydrophilicity of the surface but there is a marked improvement in the surface roughness because of the polymer film. The

improved biomolecular binding and hence the increased frequency shifts may be attributed to this improvement in the surface smoothness.

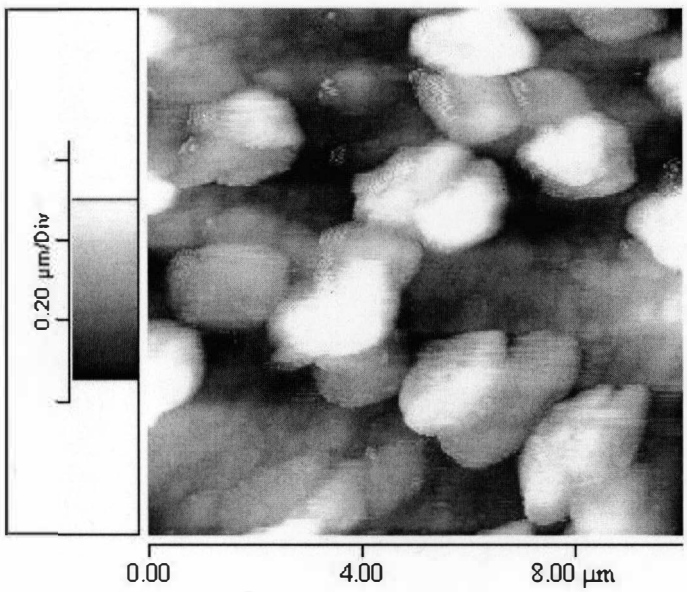

(a)

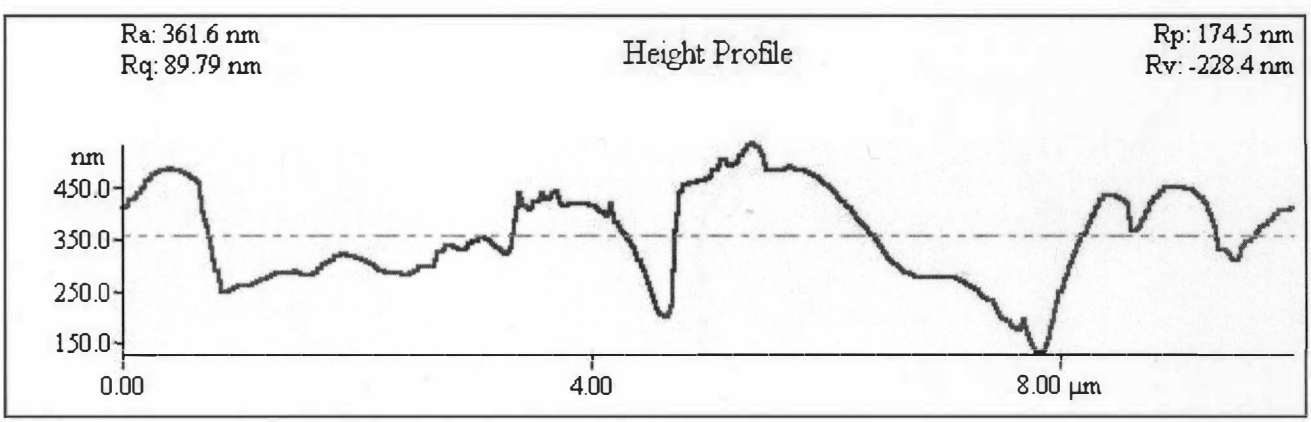

(b)

Figure 5-12: (a) AFM image of the gold surface of the QCM chip (b) Height profile of the surface along a line.

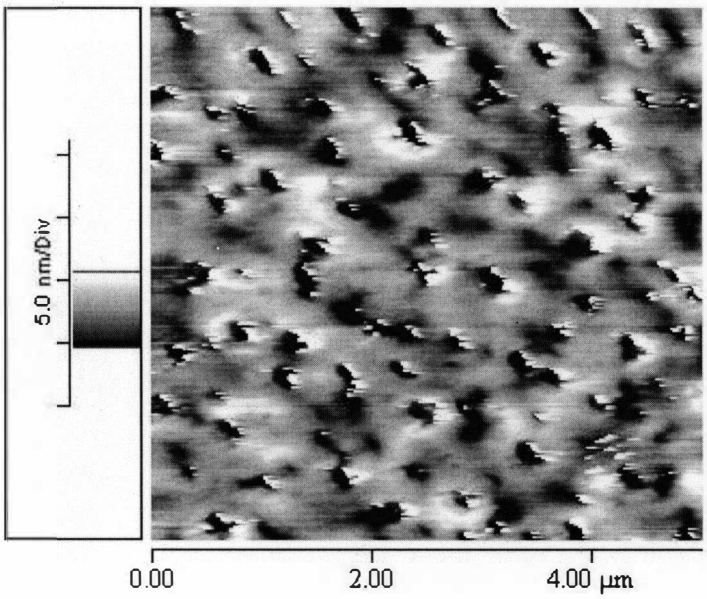

(a)

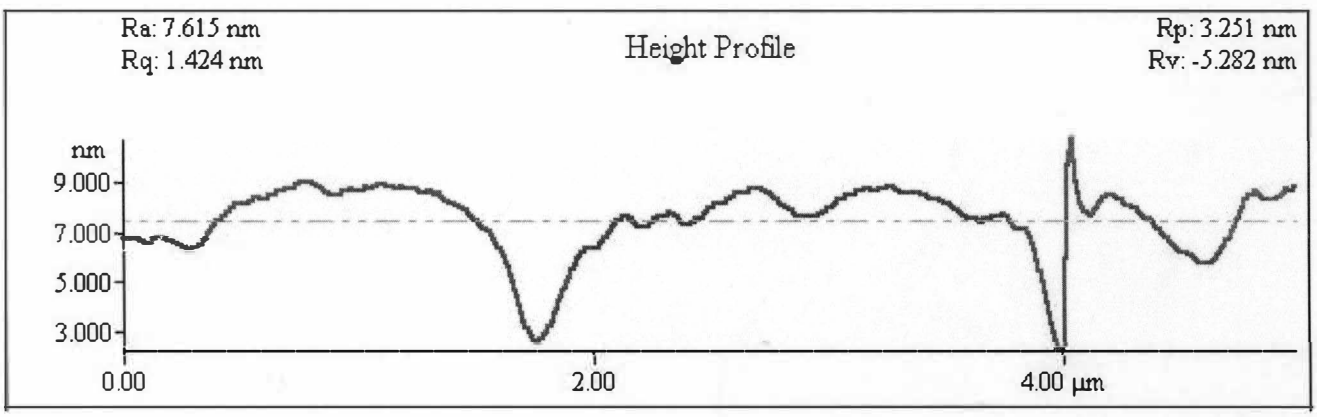

(b)

Figure 5-13: (a) AFM image of polystyrene coated gold surface and (b) Height profile of the polystyrene surface along a line.

With a surface roughness of 98.4nm, the orientation of the protein A molecules is not uniform and hence there are chances that the active sites on one protein molecule would sterically hinder the active sites on the other resulting in a non uniform binding of antibody molecules. On the other hand a polymer coated surface although decreases the

available surface area, provides the biomolecules with a much more plane and uniform surface resulting in less steric hindrance. Hence more active sites for antibody immobilization are available resulting in improved binding and hence higher sensitivity. This is pictorially represented in Figure 5-14.

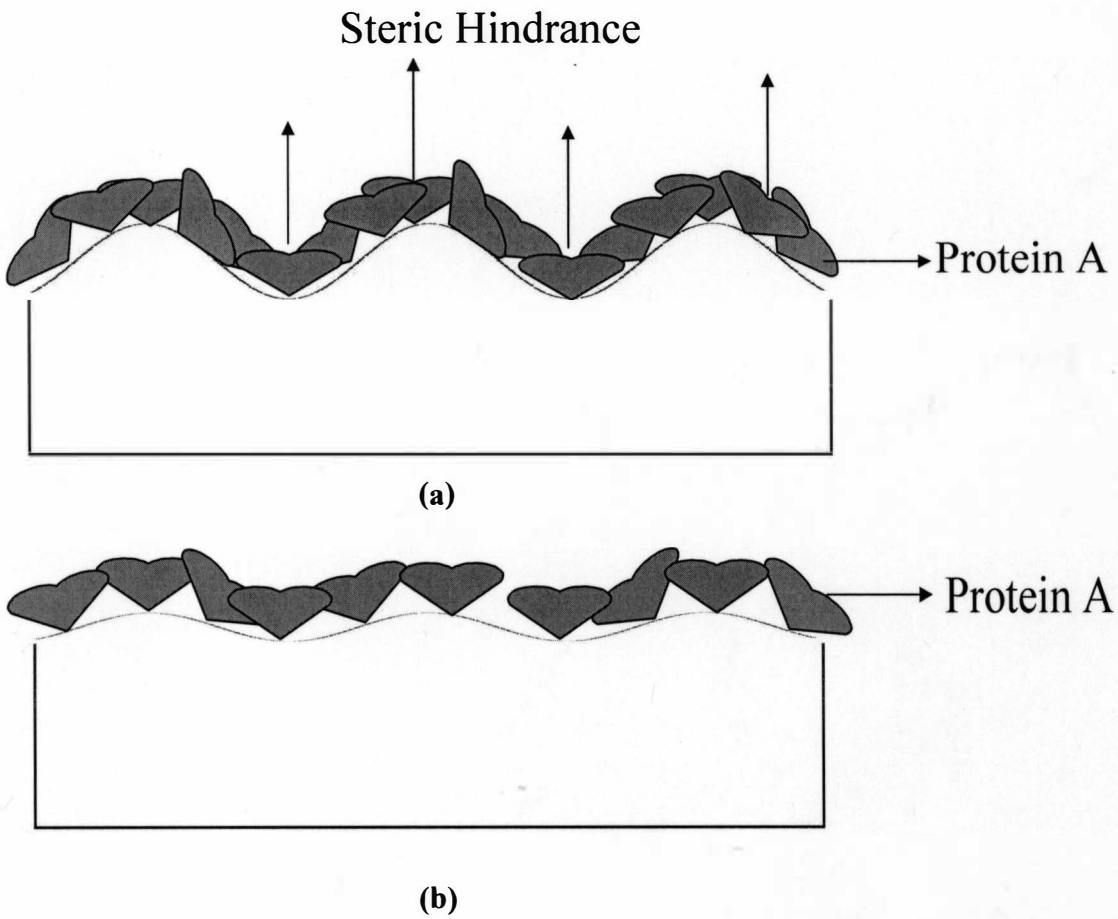

Figure 5-14: Orientation of Protein A molecules on (a) Bare gold surface resulting in steric hindrances (b) Polystyrene coated surface with reduced steric hindrance.

5.6 Summary

To determine if covering the chips with a thin polymer film could also increase the efficiency of Protein A binding and hence improvement in antibody immobilization, the gold surface was coated with an ultra thin film of polystyrene. The hydrophilicity of the

polymer film was improved by acidic treatment followed by aqueous silanization. A 65% increase in the frequency shift was observed for Protein A incubation. A similar trend was observed for IgG immobilization with the increase in frequency shifts being 40% for different antibody concentrations. This improved binding of Protein A and IgG molecules is speculated to be due to the significant decrease in the roughness of the bare gold surface when coated with polystyrene.

6. SIMULATION OF THE QCM RESONATOR USING THE FINITE ELEMENT ANALYSIS APPROACH

This chapter discusses the 2-D Finite Element (2D-FE) simulation of the design parameters and the sensing phenomenon of a QCM resonator using ANSYS. The behavior of the QCM resonator was investigated by studying the acoustic wave propagation and the particle displacement through the bulk of the device. This study was then extended to experiments wherein mass was immobilized onto the resonator surface. Under such conditions a decrease in the acoustic wave velocity was observed resulting in a decrease in the resonant frequency of the device.

6.1 Finite Element Analysis (FEA)

Finite element analysis/ solution can be divided into three stages. The first stage involves defining the problem. The keypoints, nodes, areas and volumes are defined followed by the definition of the element type and its material and geometric properties. The lines, areas and volumes created are then meshed. The second stage of the analysis involves defining the loads and the constraints and solving the resulting set of equations. The final stage of the result includes post processing the results to see the nodal displacements, deflections, forces etc.

6.2 ANSYS Calculations

The equations which relate the electrical and mechanical properties of a piezoelectric substrate are

$$T = c.\ S - e.\ E \qquad (1)$$

$$D = e^{t}.\ S + \varepsilon.\ E \qquad (2)$$

where T = stress vector.

c= elasticity matrix and has a value of S_E^{-1}; where S_E is the compliance matrix.

D = Electric flux density vector.

S = strain vector.

E = electric field vector.

ε = dielectric (permittivity) matrix and has a value of $\varepsilon_T - d.\ S_E^{-1}.\ d^{t}$; where d is the piezoelectric coupling factor.

e = piezoelectric crystal stress matrix and has a value of $d.\ S_E^{-1}$.

The compliance matrix S_E for quartz is given by

$$S_E = \begin{bmatrix} 12.77 & -1.79 & -1.22 & -4.5 & 0 & 0 \\ -1.79 & 12.77 & -1.22 & 4.5 & 0 & 0 \\ -1.22 & -1.22 & 9.6 & 0 & 0 & 0 \\ -4.5 & 4.5 & 0 & 20.04 & 0 & 0 \\ 0 & 0 & 0 & 0 & 20.04 & -9 \\ 0 & 0 & 0 & 0 & -9 & 29.1 \end{bmatrix} \times 10^{-12}\ \mathrm{m^2/N}.$$

The piezoelectric coupling factor d for quartz is given by

$$d = \begin{bmatrix} -2.3 & 2.3 & 0 & -0.67 & 0 & 0 \\ 0 & 0 & 0 & 0 & 0.67 & 4.6 \\ 0 & 0 & 0 & 0 & 0 & 0 \end{bmatrix} \times 10^{-12} \text{ C/N.}$$

The relative permittivity for quartz is given by

$$\varepsilon_T / \varepsilon_0 = \begin{bmatrix} 4.52 & 0 & 0 \\ 0 & 4.52 & 0 \\ 0 & 0 & 4.68 \end{bmatrix}; \ \varepsilon_0 = 8.854 \times 10^{-12} \text{ F/m.}$$

Based on the values above, the elasticity matrix $[c]$, the piezoelectric stress matrix $[e]$ and the dielectric (permittivity) matrix $[\varepsilon]$ for quartz were calculated to be

$$[c] = \begin{bmatrix} 8.429\times10^{10} & 4.536\times10^{9} & -1.014\times10^{10} & 1.791\times10^{10} & 0 & 0 \\ 6.788\times10^{9} & 8.654\times10^{10} & 1.014\times10^{10} & -1.791\times10^{10} & 0 & 0 \\ 1.157\times10^{10} & 1.157\times10^{10} & 1.042\times10^{11} & 4.241\times10^{-8} & 0 & 0 \\ 1.74\times10^{10} & -1.841\times10^{10} & -4.552\times10^{9} & 5.794\times10^{10} & 0 & 0 \\ 0 & 0 & 0 & 0 & 5.795\times10^{10} & 1.792\times10^{10} \\ 0 & 0 & 0 & 0 & 1.792\times10^{10} & 3.991\times10^{10} \end{bmatrix}$$

$$[e] = \begin{bmatrix} -0.19 & 0.201 & 0.05 & -0.121 & 0 & 0 \\ 0 & 0 & 0 & 0 & 0.121 & 0.196 \\ 0 & 0 & 0 & 0 & 0 & 0 \end{bmatrix}$$

$$[\varepsilon] = \begin{bmatrix} 3.904\times10^{-11} & 0 & 0 \\ 0 & 3.904\times10^{-11} & 0 \\ 0 & 0 & 4.144\times10^{-11} \end{bmatrix}$$

For modeling using ANSYS, the 6 × 6 elasticity matrix defines the stiffness coefficients and has the following form

$$[c] = \begin{array}{c} \\ \text{x} \\ \text{y} \\ \text{z} \\ \text{xy} \\ \text{yz} \\ \text{xz} \end{array} \begin{array}{c} \begin{array}{cccccc} \text{x} & \text{y} & \text{z} & \text{xy} & \text{yz} & \text{xz} \end{array} \\ \begin{bmatrix} c_{11} & & & & & \\ c_{21} & c_{22} & & & & \\ c_{31} & c_{32} & c_{33} & & & \\ c_{41} & c_{42} & c_{43} & c_{44} & & \\ c_{51} & c_{52} & c_{53} & c_{54} & c_{55} & \\ c_{61} & c_{62} & c_{63} & c_{64} & c_{65} & c_{66} \end{bmatrix} \end{array}$$

This represents the IEEE standard notation. However for ANSYS this IEEE matrix has to be transformed into an ANSYS input form such that the terms $[c_{61} \quad c_{62} \quad c_{63} \quad c_{66}]$ are entered as the ANSYS **xy** row, the terms $[c_{41} \quad c_{42} \quad c_{43} \quad c_{46} \quad c_{44}]$ are entered as the ANSYS **yz** row and the terms $[c_{51} \quad c_{52} \quad c_{53} \quad c_{56} \quad c_{54} \quad c_{55}]$ are entered as the ANSYS xz row. For 2-D modeling, the elasticity matrix [c] is therefore defined as

$$[c] = \begin{bmatrix} 8.429\times10^{10} & 0 & 0 & 0 \\ 6.788\times10^{9} & 8.65\times10^{10} & 0 & 0 \\ 1.157\times10^{10} & 1.157\times10^{10} & 1.042\times10^{11} & 0 \\ 0 & 0 & 0 & 1.792\times10^{10} \end{bmatrix}$$

Similarly the 6 × 3 piezoelectric stress matrix [e] is defined as

$$[e] = \begin{array}{c} \\ \text{x} \\ \text{y} \\ \text{z} \\ \text{xy} \\ \text{yz} \\ \text{xz} \end{array} \begin{array}{c} \begin{array}{ccc} \text{x} & \text{y} & \text{z} \end{array} \\ \begin{bmatrix} e_{11} & e_{12} & e_{13} \\ e_{21} & e_{22} & e_{23} \\ e_{31} & e_{32} & e_{33} \\ e_{41} & e_{42} & e_{43} \\ e_{51} & e_{52} & e_{53} \\ e_{61} & e_{62} & e_{63} \end{bmatrix} \end{array}$$

For ANSYS simulation, the terms $[e_{61} \quad e_{62} \quad e_{63}]$ are entered as the ANSYS **xy** row, the terms $[e_{41} \quad e_{42} \quad e_{43}]$ are entered as the ANSYS **yz** row and the terms $[e_{51} \quad e_{52} \quad e_{53}]$ are entered as the ANSYS **xz** row. For 2-D modeling, the piezoelectric stress matrix [*e*] thus assumes the form

$$[e] = \begin{bmatrix} -0.19 & 0 & 0 \\ 0.201 & 0 & 0 \\ 0.05 & 0 & 0 \\ 0 & 0.196 & 0 \end{bmatrix}$$

6.3 ANSYS Simulation Results

The piezoelectric substrate defined for the simulation was quartz with a length of 0.0254 m and a thickness of 329.164 μm. Gold electrodes with a length of 0.0132 m and a thickness of 918 nm were modeled on the top and bottom surfaces of the piezoelectric substrate and the measurements were done with the top electrode representing the liquid surface of the QCM crystal. The substrate and the bottom electrode were grounded and the entire structure was meshed with a mesh element edge length of 32.91 μm. The permittivity, elasticity and the piezoelectric matrix were defined as calculated above. The density of quartz was defined as 2651 kg/m^3. A sinusoidal signal of 5 MHz frequency was then applied across the gold electrodes. Application of a voltage causes the wave to travel through the bulk of the substrate resulting in the shear displacement of the substrate. Figure 6-1 represents the shear displacement of the substrate for simulation times of 0.3 μsec and 1 μsec.

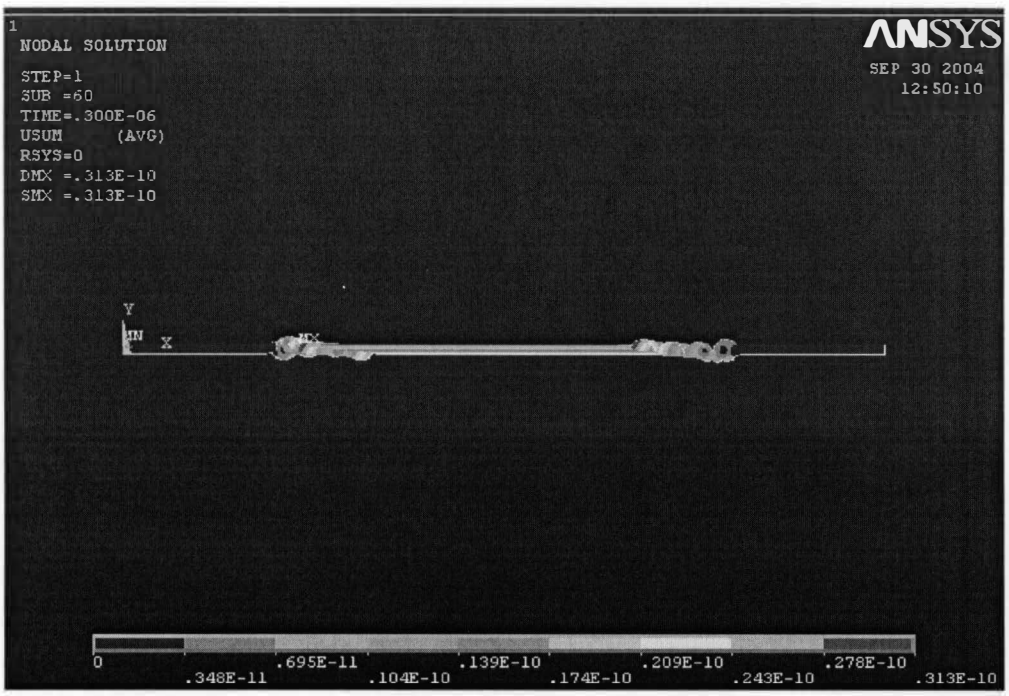

(a)

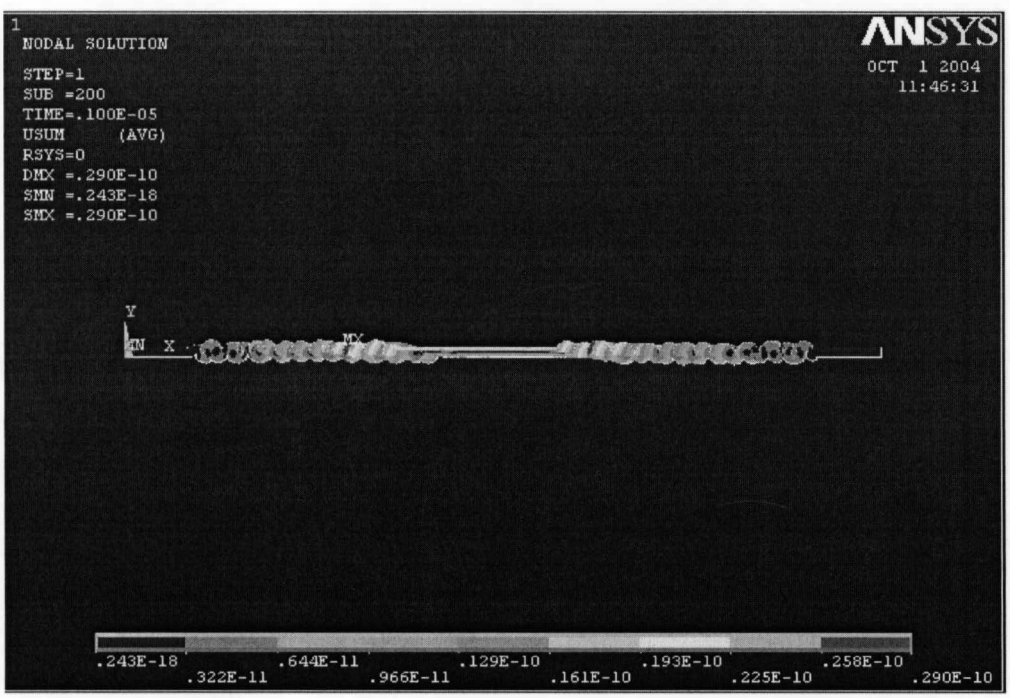

(b)

Figure 6-1: Shear displacement of the quartz substrate for simulation times of (a) 0.3 μsec (b) 1 μsec.

As the wave travels through the bulk of the substrate, it causes the particles to be displaced perpendicular to the direction of wave propagation (Y direction) along the positive and the negative X axis. The particle displacements due to the wave traveling through the quartz substrate are shown in Figure 6-2 and Figure 6-3 with the particle near the top of the surface represented by UX_2 and that in the bulk of the device represented by UX_11. A delay in the excitation time for particles in the bulk of the device (as is evident from the Figure) is because of the fact that the particle near the top surface of the substrate experiences the wave before and is therefore displaced at an earlier instant than the particle in the bulk of the device which experiences the wave at a later instant. This confirms the fact that the displacements observed for the particles is entirely due to the wave propagation through the device and not because of any potential difference between the top and the bottom surface.

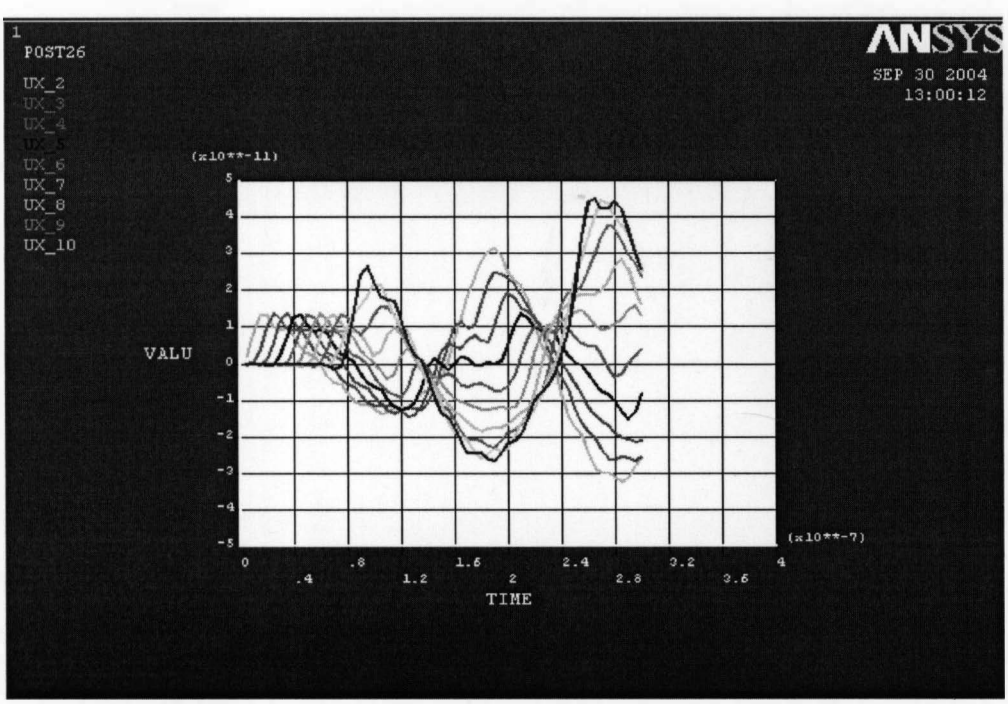

Figure 6-2: Particle displacements for simulation times of 0.3 μsec.

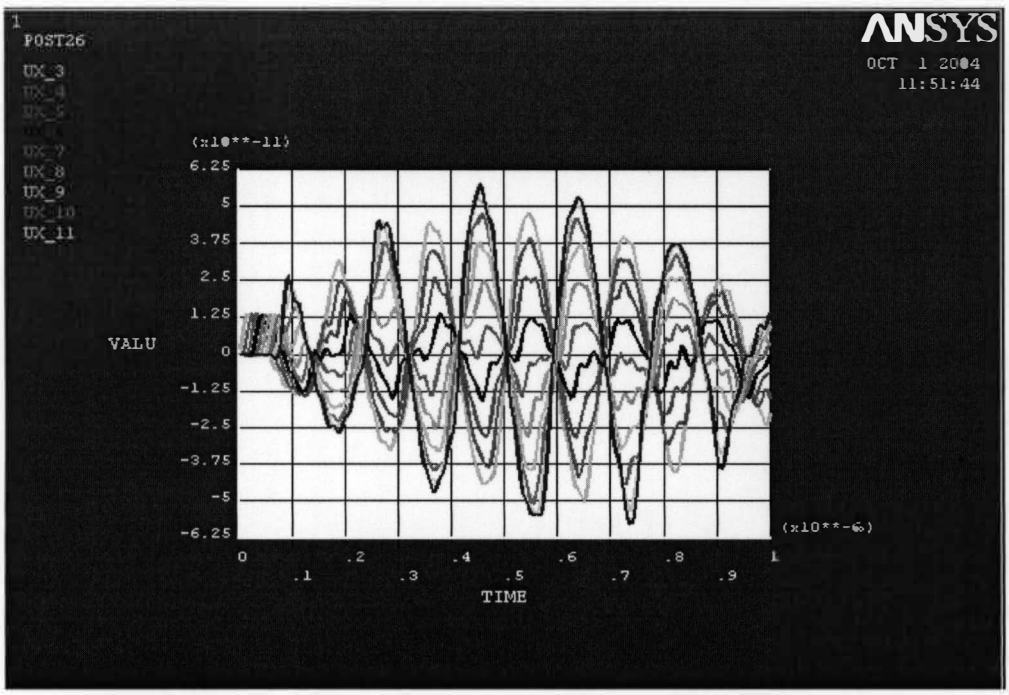

Figure 6-3: Particle displacements for simulation times of 1 μsec.

Following this a layer of polystyrene was coated onto the surface of the crystal. The thickness of the polystyrene layer coated was 5 μm. This thickness was greater than the thickness actually achieved during the experiments (35 nm) as meshing of a 35 nm thick layer was not possible. The permittivity (calculated as $k\varepsilon_0$ where k is the dielectric constant with a value of 2.4 and ε_0 is 8.854×10^{-11}), the elasticity modulus and the Poisson's ratio of the polystyrene layer were defined as 2.12×10^{-11}, 3×10^{9} and 0.35 respectively. The polymer layer, the substrate and the bottom electrode were grounded and the entire structure was meshed with a mesh element edge length of 32.91 μm. Figure 6-4 shows the particle displacements for quartz substrate coated with polystyrene for simulation times of 1μsec and 2 μsec.

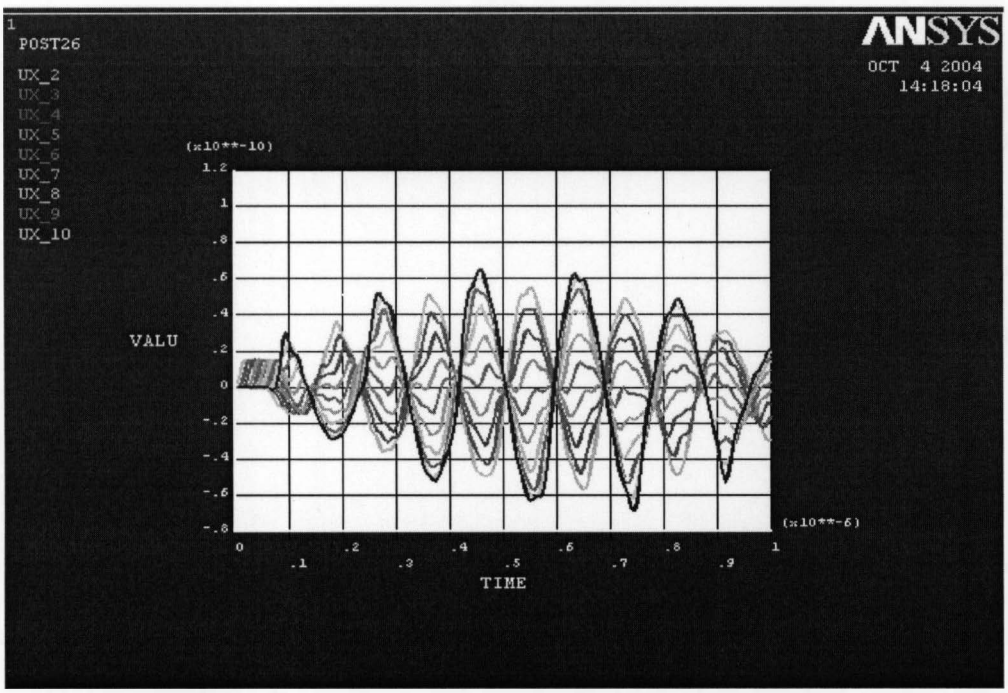

(a)

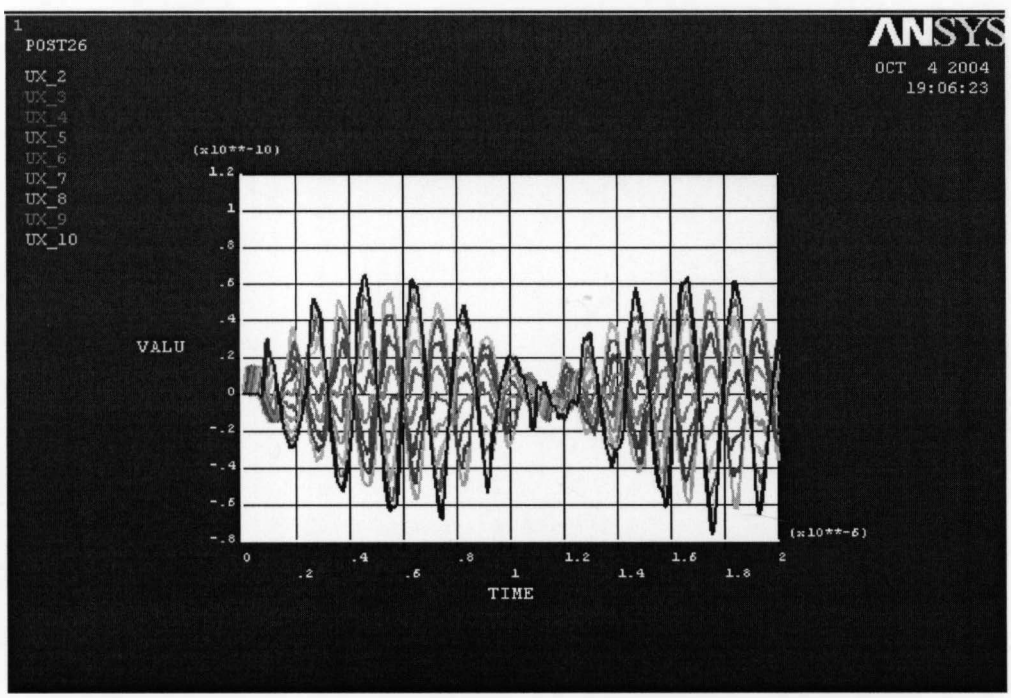

(b)

Figure 6-4: Particle displacements with polystyrene for simulation times of (a) 1 μsec (b) 2 μsec.

A zoomed image of the displacement of the bottommost particle (UX_11) for quartz and polystyrene coated quartz crystal is shown in Figure 6-5. The simulation which was done for 0.3 μseconds revealed a delay in the excitation time of the particle for the model wherein polystyrene was coated on the surface of the piezoelectric substrate. This delay was found to be 0.717 nanoseconds confirming the fact that the polymer film resulted in a decrease in the bulk wave velocity which inturn causes a shift (decrease) in the resonant frequency of the device.

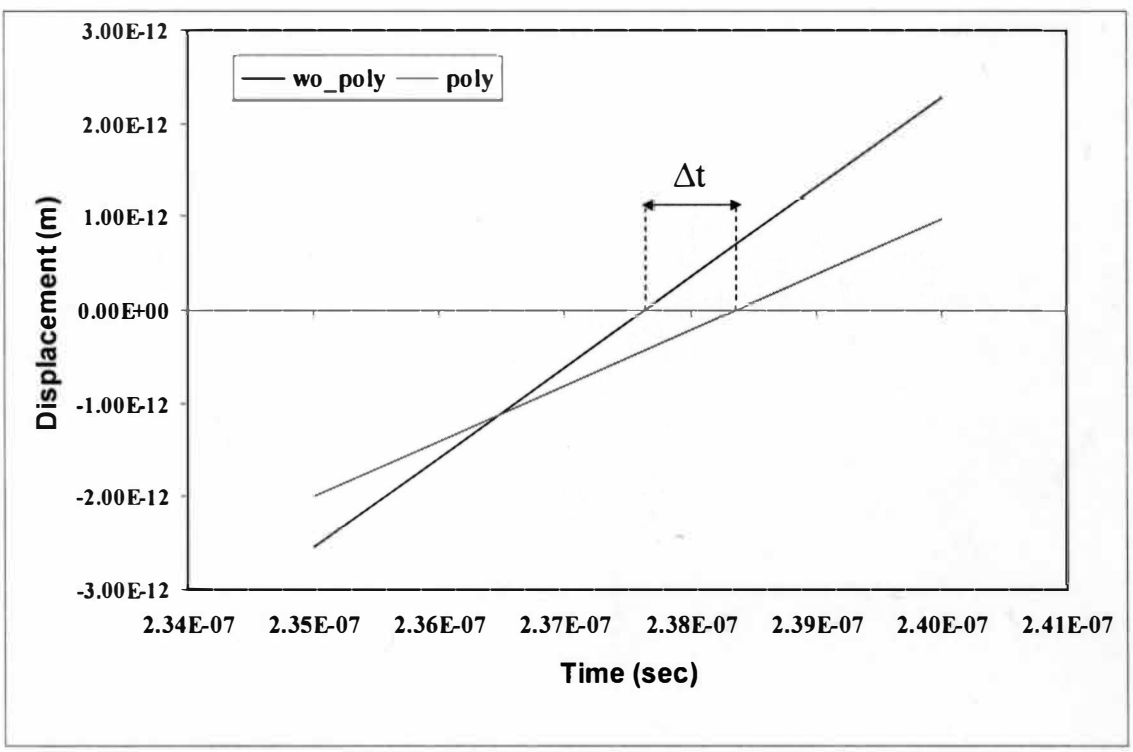

Figure 6-5: Displacement of the bottommost particle for quartz and polystyrene coated quartz substrates for simulation time of 0.3 μsec.

6.4 Calculation for the Shift in the Resonant Frequency

We know that the velocity of the acoustic wave in the bulk of the device is given by the thickness of the substrate times the resonant frequency.

$$\frac{Velocity\ of\ the\ bulk\ wave}{Thickness\ of\ the\ substrate} = Frequency \qquad (1)$$

Therefore, for a thickness of 329.164 μm and a resonant frequency of 5 MHz, the velocity of the wave can be calculated at 1645.82 m/sec. Also the time taken by the wave to traverse through the entire thickness of the substrate is given by thickness of the substrate divided by the wave velocity in that substrate.

$$\frac{Thickness\ of\ the\ substrate}{Velocity\ of\ the\ bulk\ wave} = Time\ taken\ by\ the\ wave\ to\ propagate \qquad (2)$$

For a thickness of 329.164 μm and the wave velocity of 1645.82 m/sec, the time taken by the wave to propagate the entire bulk is found to be 0.2 μsec. Since the particles in case of the polystyrene coated quartz substrate are displaced 0.717 nanoseconds after the particles in case of an uncoated device, the total time taken for the wave to propagate in the coated device is 0.2000717 μsec. Therefore the wave velocity in case of the polymer modified device is given by the thickness (329.164 μm) divided by the time (0.2000717 μsec) i. e. 1645.23 m/sec. The resonant frequency for the polystyrene coated quartz substrate is found to be 4.99 MHz. The shift in the resonant frequency on coating with a polymer film can thus be calculated to be 10 KHz (from 5 MHz to 4.99 MHz).

6.5 Confirmation of the Frequency Shift Calculated

We know that the change in the frequency (Δf) is related to the change in the mass immobilized on the surface of the sensor according to the Sauerbrey equation given by

$$\Delta f = C_f . \Delta m$$

where C_f is the sensitivity factor having a value of 0.078 Hz/ng/cm^2. From the simulation, the mass of the polystyrene layer was found to be 0.00013 grams. The frequency shift for a mass change of 0.00013 grams can be calculated as 10.14 KHz which is consistent with the simulation results.

7. CONCLUSION AND SCOPE OF FUTURE WORK

7.1 Conclusion

Owing to the increasing demands in consumer, medical and military field's development of the highly sensitive biosensors has gained utmost importance. It was demonstrated that the treatment of the QCM quartz chips with polystyrene exhibited a significant decrease in the RMS roughness of the gold crystal, resulting in a surface that was more uniform. The disadvantage of this technique, however, is that the hydrophobicity of the surface remains high. To counteract this undesirable trait, chips were treated by a simple aqueous silanization technique, which resulted in a significant improvement in the hydrophilicity of the surface. Chips that had an improved hydrophilicity were successfully utilized for biomolecular immobilization. Protein A resulted in a shift of 364 Hz on the polystyrene modified surface as opposed to the 220 Hz shift of frequency for direct immobilization (an increase of 144Hz or 65%). The results for the treated QCM chips showed 40% higher frequency shifts for different IgG concentrations as opposed to the immobilizations carried on untreated surfaces. AFM imaging revealed uniform biomolecule coverage on polymer coated surfaces. This improved binding of biomolecules when coated with polystyrene is hypothesized to be due to the marked improvement in the roughness of the surface over which the biomolecules were immobilized. Simulation and modeling of the QCM resonator was achieved using the Finite element analysis (FEA) approach in ANSYS 6.1. This simulation was used to study the behavior of the wave propagation and the particle displacement when a voltage

was applied to the QCM. Results obtained during the simulation were consistent with the experimentally achieved results.

7.2 Scope of Future Work

Following the successful immobilization of antibodies on the gold coated crystal of the QCM, my future research focuses on development of an acoustic biosensor for early detection of prostate cancer. According to the American Cancer Society Facts and Figures [56], there would be an estimated 230,110 new cases of prostate cancer in the year 2004 with around 29,900 deaths. Prostate cancer, therefore, is a considerable burden to not only those individuals that contract the disease but also to society as a whole. Being able to successfully treat prostate cancer would therefore have a significant impact on morbidity and mortality for a large group of individuals. Prostate specific antigen (PSA), a protein with a molecular weight of 33-34 KDa, has been found to be the most effective marker for diagnosis and detection of prostate cancer. The demonstrated enhancement of biomolecular immobilization achieved with functionalized polymer surfaces would be applied to the detection of PSA. Low concentrations of PSA would be detected using a Love wave acoustic sensor because of its high sensitivity and its ability to operate in a liquid environment. The future goals of the research include:

- Establishing tissue culture cells that express PSA and purify PSA from the cell culture medium.
- Transplant of tumor cells into Athymic mice by subcutaneous injection and collect blood for testing.

- Design and fabrication of Love wave acoustic sensors in a dual delay line fashion with one line acting as a sensing element and the other as a reference channel.
- Simulation and modeling of the Love wave sensor and the design of the external electronic circuitry.
- Establishing and standardizing Love wave sensor assay to detect cell culture derived PSA (PSA) with and without mass amplification.
- Establishing assay using Love wave sensor to detect total PSA (tPSA) in the serum from mice injected with tumor cells.

REFERENCES

1. S. W. Wenzel and R. M. White, "Analytical comparison of the sensitivities of bulk wave, surface wave and flexural plate wave ultrasonic gravimetric sensors", Applied Physics Letters, Vol. 54, No. 20, pp 1976, 1989.
2. G. Sauerbrey, Zeitschrift Fur Physik Vol. 155, pp 206, 1959.
3. C. Barnes, C. D'Silva, J. P. Jones, T. J. Lewis, "Lectin coated piezoelectric crystal biosensors, Sensors and Actuators B: Chemical, Vol. 7, No. 1-3, pp 347, 1992.
4. S. Imai, H. Mizuno, M. Suzuki, T. Takeuchi, E. Tamiya, F. Mashige, A. Ohkubo, I. Karube, "Total urinary protein sensor based on a piezoelectric quartz crystal", Analytica Chimica Acta, Vol. 292, No. 1-2, pp 65, 1994.
5. H. Muramatsu, J. M. Dicks, E. Tamiya, I. Karube, "Piezoelectric Crystal Biosensor Modified with Protein A for Determination of Immunoglobulins", Analytical Chemistry, Vol. 59, No. 23, pp 2760, 1987.
6. F. Caruso, E. Rodda, D. N. Furlong, "Orientational Aspects of Antibody Immobilization and Immunological Activity on Quartz Crystal Microbalance Electrodes", Journal of Colloid and Interface Science, Vol. 178, No. 1, pp 104, 1996.
7. B. Guo, J. Anzai, T. Osa, "Adsorption Behavior of Serum Albumin on Electrode Surfaces and the Effects of Electrode Potential", Chemical & Pharmaceutical Bulletin, Vol. 44, No. 4, pp 800, 1996.
8. S. P. Sakti, P. Hauptmann, B. Zimmermann, F. Buhling, S. Ansorge, "Disposable HSA QCM-immunosensor for practical measurement in liquid", Sensors & Actuators B: Chemical, Vol. 78, No. 1-3, pp 257, 2001.
9. R. M. White and F. W. Voltmer, "Direct piezoelectric coupling to surface elastic waves", Applied Physics Letters, Vol. 7, No. , pp 314, 1965.
10. C. Y. Shen, C. P. Huang, W. T. Huang, "Gas-detecting properties of surface acoustic wave ammonia sensors", Sensors and Actuators B: Chemical, Vol. 101, No. 1-2, pp 1, 2004.
11. O. K. Varghese, D. Gong, W. R. Dreschel, K. G. Ong, C. A. Grimes, "Ammonia detection using nanoporous alumina resistive and surface acoustic wave sensors", Sensors and Actuators B: Chemical, Vol. 94, No. 1, pp 27, 2003.
12. J. Fontecha, M. J. Fernández, I. Sayago, J. P. Santos, J. Gutiérrez, M. C. Horrillo, I. Gràcia, C. Cané and E. Figueras, "Fine-tuning of the resonant frequency using a hybrid coupler and fixed components in SAW oscillators for gas detection", Sensors and Actuators B: Chemical, Vol. 103, No. 1-2, pp 139, 2004.
13. N. Barié and M. Rapp, "Covalent bound sensing layers on surface acoustic wave (SAW) biosensors", Biosensors and Bioelectronics, Vol. 16, No. 9-12, pp 979, 2001.

14. E. Howe and G. Harding, "A comparison of protocols for the optimisation of detection of bacteria using a surface acoustic wave (SAW) biosensor", Biosensors and Bioelectronics, Vol. 15, No. 11-12, pp 641, 2000.

15. T. Wessa, M. Rapp, H. J. Ache, "New immobilization method for SAW-biosensors: covalent attachment of antibodies via CNBr", Biosensors and Bioelectronics, Vol. 14, Issue 1, pp 93, 1999.

16. J. Kondoh, Y. Matsui, S. Shiokawa, W. B. Wlodarski, "Enzyme-immobilized SH-SAW biosensor", Sensors and Actuators B: Chemical, Vol. 20, No. 2-3, pp 199, 1994.

17. F. Martin , M. I. Newton , G. McHale , K. A. Melzak, E. Gizeli, "Pulse mode shear horizontal-surface acoustic wave (SH-SAW) system for liquid based sensing applications" Biosensors and Bioelectronics, Vol. 19, No. 6, pp 627, 2004.

18. T. Nomura, A. Saitoh, T. Miyazaki, "Liquid sensor probe using reflecting SH-SAW delay line", Sensors and Actuators B: Chemical, Vol. 91, No. 1-3, pp 298, 2003.

19. C. Déjous, M. Savart, D. Rebière, J. Pistré, "A shear-horizontal acoustic plate mode (SH-APM) sensor for biological media", Sensors and Actuators B: Chemical, Vol. 27, No. 1-3, pp 452, 1995.

20. I. Esteban, C. Déjous, D. Rebière, J. Pistré, R. Planade, J. F. Lipskier, "Mass sensitivity of SH-APM sensors: potentialities for organophosphorous vapors detection", Sensors and Actuators B: Chemical, Vol. 68, No. 1-3, pp 244, 2000.

21. E. Gizelli, N. J. Goddard, C. R. Lowe, A. C. Stevenson, "A Love plate biosensor utilizing a polymer layer", Sensors and Actuators B: Chemical, Vol. 6, No. 1-3 , pp 131, 1992.

22. F. Josse, F. Bender, R. W. Cernosek, "Guided shear horizontal surface acoustic wave sensors for chemical and biochemical detection in liquids", Analytical Chemistry, Vol. 73, No. 24 , pp 5937, 2001.

23. G. L. Harding, "Mass Sensitivity of love-mode acoustic sensors incorporating silicon dioxide and silicon-oxy-fluoride guiding layers", Sensors and Actuators A: Physical, Vol. 88, No. 1, pp 20, 2001.

24. J. Du, G. L. Harding, J. A. Ogilvy, P. R. Drencher, M. Lake, "A study of love wave acoustic sensors", Sensors and Actuators A: Physical, Vol. 56, No. 3, pp 211, 1996.

25. G. L. Harding, J. Du, P. R. Dencher, D. Barnett, E. Howe, "Love wave acoustic immunosensor operating in liquid", Sensors and Actuators A: Physical, Vol. 61, No. 1-3, pp 279, 1996.

26. E. Gizelli, "Study of the sensitivity of the acoustic waveguide sensor" Analytical Chemistry, Vol. 72, No. 24, pp 5967, 2000.

27. K. K. Zadeh, A. Trinchi, W. Wlodarski, A. Holland, "A novel love-mode device based on a ZnO/ ST-cut quartz crystal structure for sensing applications", Sensors and Actuators A: Physical, Vol. 100, No. 2-3, pp 135, 2002.

28. A. W. Wang, R. Kiwan, R. M. White, R. L. Ceriani, "A silicon-based ultrasonic immunoassay for detection of breast cancer antigens", Sensors and Actuators B: Chemical, Vol. 49, No. 1-2, pp 13, 1998.

29. G. Kovacs and A. Venema, "Theoretical comparison of sensitivities of acoustic shear wave modes for (bio) chemical sensing in liquids", Applied Physics Letters, Vol. 61, No. 6, pp 639, 1992.

30. F. Legay, S. Gauron, F. Deckert, G. Gosset, U. Pfaar, C. Ravera, H. Wiegand , H. Schran, "Development and validation of a highly sensitive RIA for zoledronic acid, a new potent heterocyclic bisphosphonate, in human serum, plasma and urine", Journal of Pharmaceutical and Biomedical Analysis, Vol. 30, No. 4, pp 897, 2002.

31. A. W. Wang, R. Kiwan, R.M. White, R. L. Ceriani, "A silicon-based ultrasonic immunoassay for detection of breast cancer antigens", Sensors and Actuators B: Chemical, Vol. 49, No. 1-2, pp 13, 1998.

32. C. Paepens, S. D. Saeger, L. Sibanda, I. B. Vetró, I. Léglise, F. V. Hove, C. V. Peteghem, "A flow-through enzyme immunoassay for the screening of fumonisins in maize", Analytica Chimica Acta, Vol. 523, No. 2, pp 229, 2004.

33. P. F. Bolado, M. B. G. García, A. C. García, "Voltammetric determination of alkaline phosphatase and horseradish peroxidase activity using 3-indoxyl phosphate as substrate: Application to enzyme immunoassay", Talanta, Vol. 64, No. 2, pp 452, 2004.

34. W. Zhan, X. Wang, J. Chen, J. Xing, H. Fukuda, "Elimination of shrimp endogenous alkaline phosphatase background and development of enzyme immunoassays for the detection of white spot syndrome virus (WSSV)", Aquaculture, Vol. 239, No. 1-4, pp 15, 2004.

35. J. Fiet, F. Giton, I. Fidaa, A. Valleix, H. Galons, J.P. Raynaud, "Development of a highly sensitive and specific new testosterone time-resolved fluoroimmunoassay in human serum", Steroids, Vol. 69, No. 7, pp 461, 2004.

36. W. Yang, C. G. Zhang, H. Y. Qu, H. H. Yang, J. G. Xu, "Novel fluorescent silica nanoparticle probe for ultrasensitive immunoassays", Analytica Chimica Acta, Vol. 503, No. 2, pp 163, 2004.

37. N. Yamamoto, H. Hasegawa, H. Seki, K. Ziegelbauer, T. Yasuda, "Development of a high-throughput fluoroimmunoassay for Syk kinase and Syk kinase inhibitors", Analytical Biochemistry, Vol. 315, No. 2, pp 256, 2003.

38. J. Lin, F. Yan, X. Hu, H. Ju, "Chemiluminescent immunosensor for CA19-9 based on antigen immobilization on a cross-linked chitosan membrane", Journal of Immunological Methods, Vol. 291, No. 1-2, pp 165, 2004.

39. H. S. Zhuang, J. L. Huang, G. N. Chen, "Synthesis of a new biacridine and its use as the chemiluminescent probe for immunoassay of carcinoembryonic antigen", Analytica Chimica Acta, Vol. 512, No. 2, pp 347, 2004.

40. Y. Dotsikas and Y. L. Loukas, "Employment of 4-(1-imidazolyl)phenol as a luminol signal enhancer in a competitive-type chemiluminescence immunoassay and its comparison with the conventional antigen–horseradish peroxidase conjugate-based assay", Analytica Chimica Acta, Vol. 509, No. 1, pp 103, 2004.

41. G. L. Harding, J. Du, P. R. Dencher, D. Barnett, E. Howe, "Love wave acoustic immunosensor operating in liquid", Sensors and Actuators A: Physical, Vol. 61, No. 1-3, pp 279, 1996.

42. Y. Y. Wong, S. P. Ng, M. H. Ng, S. H. Si, S. Z. Yao, Y. S. Fung, "Immunosensor for the Differentiation and Detection of Salmonella Species Based on a Quartz Crystal Microbalance", Biosensors & Bioelectronics, Vol. 17, No. 8, pp 676, 2002.

43. J. W. Grate, S. J. Martin, R. M. White, "Acoustic Wave Microsensors Part I", Analytical Chemistry, Vol. 65, No. 21, pp 940A, 1993.

44. G. Sauerbrey, Zeitschrift Fur Physik Vol. 155, pp 206, 1959.

45. P. H. Justesen, T. Kristensen, T. Ebdrup, D. Otzen, "Investigating porcine pancreatic phospholipase A_2 action on vesicles and supported planar bilayers using a quartz crystal microbalance with dissipation", Journal of Colloid and Interface Science, Vol. 279, No. 2, pp 399, 2004.

46. Y. Liu, W. Zhang, X. Yu, H. Zhang, R. Zhao, D. Shangguan, Y. Li, B. Shen, G. Liu, "Quartz crystal biosensor for real-time kinetic analysis of interaction between human TNF-α and monoclonal antibodies", Sensors and Actuators B: Chemical, Vol. 99, No. 2-3, pp 416, 2004.

47. Y. Liu, X. Yu, R. Zhao, D.Shangguan, Z. Bo, G. Liu, "Quartz crystal biosensor for real-time monitoring of molecular recognition between protein and small molecular medicinal agents", Biosensors and Bioelectronics, Vol. 19, No. 1, pp 9, 2003.

48. I. Mannelli, M. Minunni, S. Tombelli, M. Mascini, "Quartz crystal microbalance (QCM) affinity biosensor for genetically modified organisms (GMOs) detection", Biosensors and Bioelectronics, Vol. 18, No. 2-3, pp 129, 2003.

49. G. Binnig, C. F. Quate, Ch. Gerber, "Atomic Force Microscope", Physical Review Letters, Vol. 56, No. 9, pp 930, 1986.

50. H. Muramatsu, J. M. Dicks, E. Tamiya, I. Karube, "Piezoelectric Crystal Biosensor Modified with Protein A for Determination of Immunoglobulins" Analytical Chemistry, Vol. 59, No. 23, pp 2760, 1987.

51. T. Nomura and M. Okuhara, "Frequency shifts of piezoelectric quartz crystals immersed in organic liquids", Analytica Chimica Acta, Vol. 142, pp 281, 1982.

52. K. Keiji Kanazawa and Joseph G. Gordon, II, "The oscillation frequency of a quartz resonator in contact with liquid", Analytica Chimica Acta, Vol. 175, pp 99, 1985.

53. J. Buijs, J. W. T. Lichtenbelt, W. Norde, J. Lyklema, "Adsorption of monoclonal IgGs and their $F(ab')_2$ fragments onto polymeric surfaces", Colloids and Surfaces B: Biointerfaces, Vol. 5, No. 1-2, pp 11, 1995.

54. N. Zammatteo, C. Girardeaux, D. Delforge, J. J. Pireaux, J. Remacle, «Amination of Polystyrene Microwells: Application to the Covalent Grafting of DNA Probes for Hybridization Assays", Analytical Biochemistry, Vol. 236, No. 1, pp 85, 1996.

55. J. Kaur, K. V. Singh, M. Raje, G. C. Varshney, C. R. Suri, "Strategies for direct attachment of hapten to a polystyrene support for applications in enzyme-linked immunosorbent assay (ELISA)", Analytica Chimica Acta, Vol. 506, No. 2, pp 133, 2004.

56. [Available Online], "Cancer Facts & Figures, 2004", American Cancer Society, http://www.cancer.org/downloads/STT/CAFF_finalPWSecured.pdf.